Tectonic Significance of Upper Cambrian–Middle Ordovician Mafic Volcanic Rocks on the Alexander Terrane, Saint Elias Mountains, Northwestern Canada
Author(s): Luke P. Beranek, Cees R. van Staal, Sarah M. Gordee, William C. McClelland, Steve Israel, Mitchell Mihalynuk
Reviewed work(s):
Source: *The Journal of Geology*, Vol. 120, No. 3 (May 2012), pp. 293-314
Published by: The University of Chicago Press
Stable URL: http://www.jstor.org/stable/10.1086/664788
Accessed: 01/05/2012 03:41

Tectonic Significance of Upper Cambrian–Middle Ordovician Mafic Volcanic Rocks on the Alexander Terrane, Saint Elias Mountains, Northwestern Canada

Luke P. Beranek,[1,*] *Cees R. van Staal,*[1] *Sarah M. Gordee,*[2] *William C. McClelland,*[3] *Steve Israel,*[4] *and Mitchell Mihalynuk*[5]

1. Geological Survey of Canada, 625 Robson Street, Vancouver, British Columbia V6B 5J3, Canada; 2. University of Tasmania, Hobart, Tasmania, Australia; 3. University of Iowa, Iowa City, Iowa, U.S.A.; 4. Yukon Geological Survey, Whitehorse, Yukon, Canada; 5. British Columbia Geological Survey, Victoria, British Columbia, Canada

ABSTRACT

Upper Cambrian to Middle Ordovician mafic volcanic rocks of the Donjek assemblage comprise the oldest exposed units of the Alexander terrane in the Saint Elias Mountains of northwestern Canada. In this study, we use the geochemical and geological characteristics of these rocks to decipher their tectonic setting, petrogenetic history, and relationship to the early Paleozoic Descon arc system of the Alexander terrane in southeastern Alaska. Donjek assemblage volcanic rocks are subdivided into three geochemical types: transitional basalt (type I), light rare earth–enriched island-arc tholeiite to calc-alkaline basalt (type II), and enriched mid-ocean ridge basalt to ocean-island basalt (type III). Simple petrogenetic models illustrate that the basalts were generated by the decompressional partial melting of enriched asthenospheric mantle and variably mixed with depleted mantle and subduction-related components. Analogous geochemical signatures for modern Sumisu Rift and Okinawa Trough lavas imply that the Donjek assemblage basalts erupted during the rifting of the Descon arc. This model provides a new comparative framework for terranes of Siberian, Baltican, and Caledonian affinity in the North American Cordillera and, in particular, suggests a paleogeographic connection to rift-related magmatism in the Seward Peninsula region of the Arctic Alaska–Chukotka terrane.

Online enhancements: appendix tables.

Introduction

The North American Cordillera is the classic example of an accretionary orogen and is mostly composed of fault-bounded crustal fragments, or terranes, added to the western margin of Laurentia (ancestral North America) since the late Paleozoic (e.g., Coney et al. 1980; Monger and Nokelberg 1996; Cawood et al. 2009). There is a growing consensus that the North American Cordillera is subdivided into distinct lithotectonic realms (fig. 1), each of which contains interrelated terranes with similar basement domains, magmatic histories, and faunal provincialities (Colpron et al. 2007; Colpron and Nelson 2009). Some of the most outstanding problems in orogen evolution concern a group of terranes in the western Cordillera with Neoproterozoic to early Paleozoic underpinnings (Alexander, Arctic Alaska–Chukotka, Farewell, and others; e.g., Gehrels and Saleeby 1987*a*; Decker et al. 1994; Patrick and McClelland 1995; Lindsley-Griffin et al. 2008; Amato et al. 2009). Although the original positions of these terranes are unknown, the available fossil evidence suggests that they had larval exchange with the paleocontinents of Laurentia, Baltica (the ancestral European craton), and Siberia during the early to mid-Paleozoic (e.g., Soja 1994, 2008; Blodgett et al. 2002; Dumoulin et al. 2002). Paleomagnetic and sedimentary provenance data further imply that some of these terranes had mid-Paleozoic locations proximal to the northern Cal-

Manuscript received February 15, 2011; accepted December 15, 2011.

* Author for correspondence; e-mail: luke.beranek@gmail.com; luke.beranek@geo.su.se.

[The Journal of Geology, 2012, volume 120, p. 293–314]
0022-1376/2012/12003-0003$15.00. DOI: 10.1086/664788

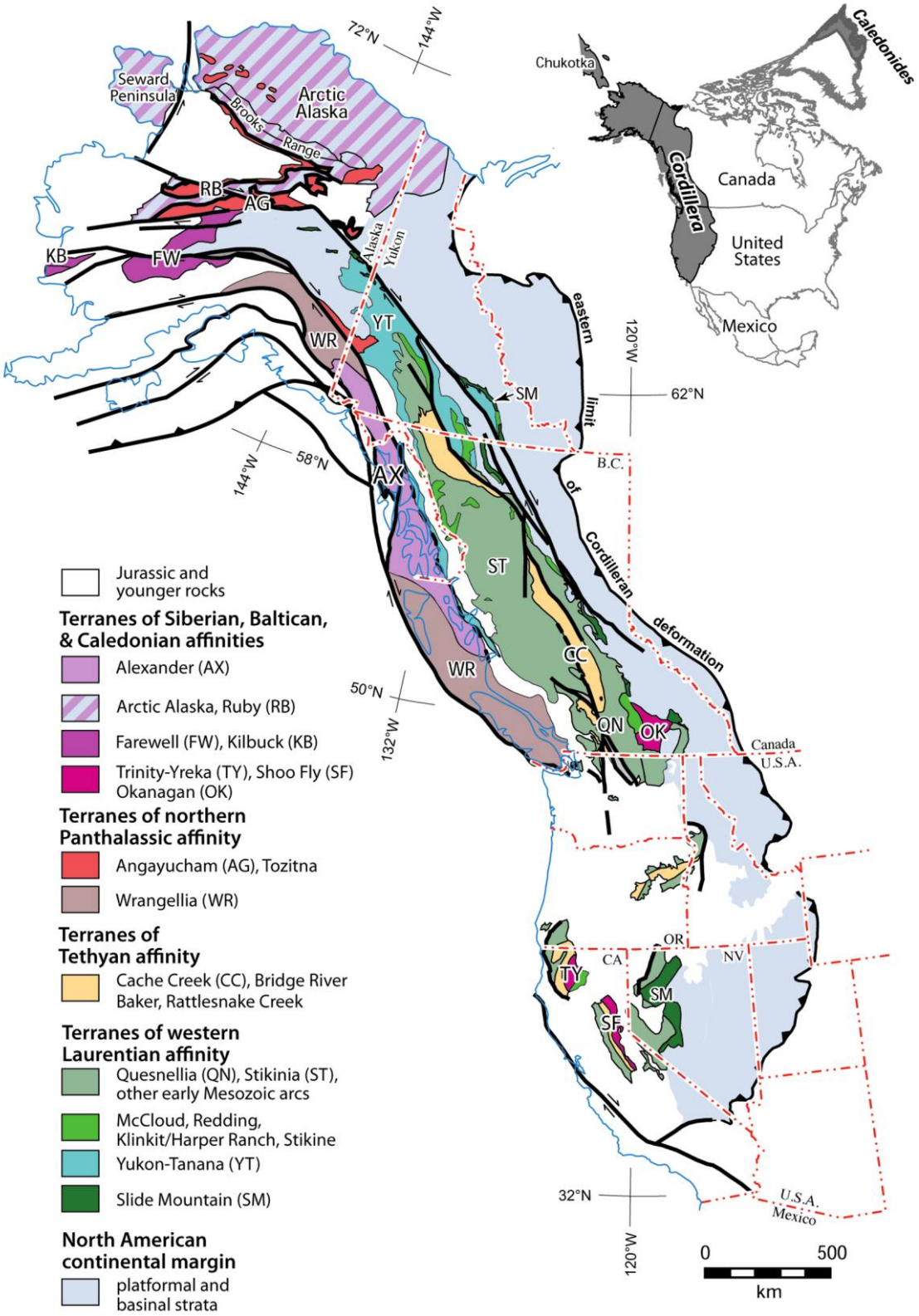

Figure 1. Paleozoic to early Mesozoic terranes of the North American Cordillera, modified from work by Colpron and Nelson (2009). Terranes are grouped according to faunal affinity and interpreted positions in early Paleozoic time. B.C. = British Columbia; CA = California; OR = Oregon; NV = Nevada; U.S.A. = United States of America.

edonian orogenic belt of Greenland, Scandinavia, and the British Isles (Bazard et al. 1995; Bradley et al. 2007; Amato et al. 2009). Colpron and Nelson (2009) assigned most of the western Cordilleran terranes to the Siberian-Baltican-Caledonian lithotectonic realm (fig. 1).

The Alexander terrane is a crustal fragment that underlies ~100,000 km^2 of the western Cordillera in southeastern Alaska; the Saint Elias Mountains of eastern Alaska, southwestern Yukon, and northwestern British Columbia; and the coastal region of west-central British Columbia (fig. 1). Many fundamental questions remain about the geological evolution of the Alexander terrane and its association with other terranes in the Siberian-Baltican-Caledonian lithotectonic realm (Wright and Wyld 2006; Grove et al. 2008; Soja and Krutikov 2008; Colpron and Nelson 2009; Miller et al. 2011). Central to these questions are the origin and tectonic significance of early Paleozoic magmatic rocks that cover and intrude the Neoproterozoic basement of the Alexander terrane. Upper Cambrian to Middle Ordovician mafic volcanic and marine sedimentary rocks of the Donjek assemblage, the oldest exposed strata in the Saint Elias Mountains, provide an excellent opportunity to investigate the setting of early Paleozoic magmatism. In this article, we present and interpret the geochemical and geological characteristics of Donjek assemblage volcanic rocks to understand their mantle sources, petrogenetic history, and relationship to lower Ordovician to Silurian arc-type volcanic strata of the Descon Formation on the southern Alexander terrane of southeastern Alaska. The comparison of our data with those from modern volcanic rocks in the western Pacific Ocean suggests that the Donjek assemblage records the rifting of the Descon arc. The tectonic setting of the Donjek assemblage leads us to propose new ideas about the early Paleozoic paleogeography of the Alexander terrane and its geological connections with other terranes of Siberian, Baltican, and Caledonian affinity in the North American Cordillera.

Tectonic and Paleogeographic Framework

The Alexander terrane is a composite tectonic element (Berg et al. 1978) divided (as modified by Gehrels and Saleeby 1987*a*) into two crustal fragments—the Craig and Admiralty subterranes—on the basis of apparent differences in their early stratigraphic, magmatic, and tectonic records. Geological and geochronological evidence supports Late Pennsylvanian to Early Permian tectonic juxtaposition of the subterranes (Karl et al. 2010), an event that may be linked to the amalgamation of the Alexander, Wrangellia, and Peninsular terranes (van Staal et al. 2010).

Craig Subterrane. The Craig subterrane underlies more than 90% of the Alexander terrane in southeastern Alaska, the Saint Elias Mountains, and west-central British Columbia (fig. 2). In the Prince of Wales Island region of southeastern Alaska, metasedimentary and arc-type meta-igneous rocks of the Wales Group constitute the basement of the Craig subterrane (fig. 3). An Ediacaran depositional age for the Wales Group is constrained by a felsic metavolcanic unit on Prince of Wales Island dated by U-Pb zircon at 595 ± 20 Ma (Gehrels et al. 1996). An orthogneiss body that intrudes the metavolcanic succession on nearby Dall Island yields a U-Pb zircon age of 554 ± 4 Ma (Gehrels 1990). Paleozoic strata conceal the Neoproterozoic basement in the Saint Elias Mountains; however, plutons in the Chilkat Range (fig. 2) northwest of Haines, Alaska, contain 544-Ma xenocrystic zircons sourced from underlying rocks similar in age to the Wales Group (Karl et al. 2006). Rocks of the Wales Group were penetratively deformed and metamorphosed to greenschist- to amphibolite-facies during latest Neoproterozoic to Cambrian time, an event Gehrels and Saleeby (1987*a*) termed the Wales orogeny (fig. 3).

The Wales Group forms the depositional basement of the Descon Formation in the Prince of Wales Island region (fig. 3). The dominant lithologies of this formation include mafic to felsic lava, volcaniclastic rocks, shale, and limestone (Eberlein and Churkin 1970). Calc-alkaline intrusive rocks coeval with the Descon Formation consist of quartz diorite, quartz monzonite, and granodiorite (Gehrels and Saleeby 1987*b*). The lower Descon Formation contains volcanogenic massive sulfide (VMS) deposits that illustrate "Kuroko-type" mineralization (Slack et al. 2006; Nelson et al. 2010), which may indicate exhalation in a tectonic environment analogous to volcanic arc-rift successions in the Kuroko district of Honshu, Japan. Although flare-up of the Descon arc was originally reported to have commenced by Early to Middle Ordovician time (e.g., Gehrels and Saleeby 1987*a*, using the timescale of Palmer 1983), 497–488-Ma detrital zircons in Descon Formation sandstone imply that subduction-related magmatism had begun by the Late Cambrian (Grove et al. 2008, using the timescale of Gradstein et al. 2004). The Descon arc system is interpreted to have faced southwest (present coordinates), with Paleozoic strata of the Saint

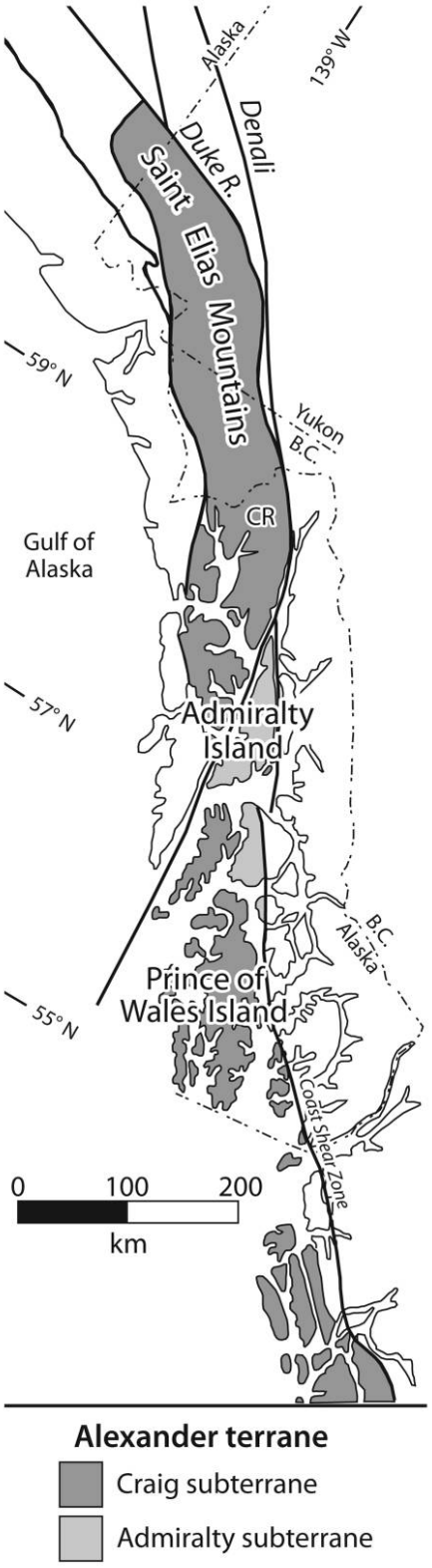

Figure 2. Location map of the Craig and Admiralty subterranes of the Alexander terrane. B.C. = British Columbia; CR = Chilkat Range; R. = river.

Elias Mountains deposited behind the arc in a shallow- to deepwater basin (Gehrels and Saleeby 1987*a*).

Silurian shallow-water marine strata of the Heceta Formation conformably overlie the Descon Formation (e.g., Soja 1990). Distinctive stromatolite-sphinctozoan reef faunas of this formation are thought to provide a paleogeographic connection between the Craig subterrane and rocks in the Ural Mountains of present-day Eurasia (Soja 1994; Soja and Antoshkina 1997). Conglomeratic sequences in the upper parts of the Heceta Formation document the earliest phases of the Klakas orogeny, a regional event characterized by thrust faulting, greenschist- to amphibolite-facies metamorphism, and intrusion of trondhjemite and garnet-bearing plutons (Gehrels and Saleeby 1987*a*). The Klakas orogeny culminated with the deposition of Upper Silurian and Devonian red beds of the Karheen Formation (fig. 3), an 1800-m-thick molasse succession dominated by terrigenous to shallow-marine siliciclastic rocks (Eberlein and Churkin 1970). Karheen Formation sandstone is composed of detrital zircons with ages that cluster at 412–491, 1011–1440, 1485–1613, and 1722–2892 Ma (Grove et al. 2008). The Paleozoic-age zircons are consistent with sources from the Descon arc, whereas the Precambrian zircons imply derivation from an unknown continental block involved in the Klakas orogeny (Gehrels et al. 1996). Paleomagnetic data from the Karheen Formation require the Craig subterrane to be located at 14° ± 5° (north or south) paleolatitude during the Early Devonian (Bazard et al. 1995). Combining the record of igneous and orogenic events, faunal affinities, and the lithologic character of Karheen red beds, Bazard et al. (1995) favored a Northern Hemisphere position near the Scandinavian Caledonides.

Admiralty Subterrane. The Admiralty subterrane predominantly underlies the Admiralty Island region of southeastern Alaska (fig. 2). Basement rocks on Admiralty Island consist of biotite chlorite, actinolite, and graphitic schist of the Retreat Group (Gehrels and Berg 1992). Metaplutonic rocks that intrude the schist units yield U-Pb zircon ages of 545–547 Ma (Karl et al. 2006). The Hood Bay Formation is a basinal assemblage of radiolarian chert, argillite, graywacke, limestone, and pillow basalt that overlies the Retreat Group. The depositional age of the Hood Bay Formation is constrained by black argillite that yields Middle to Late Ordovician graptolites of the *Climacograptus bicornis* zone (Carter 1977). The Devonian to Permian record of the Admiralty subterrane consists of chert,

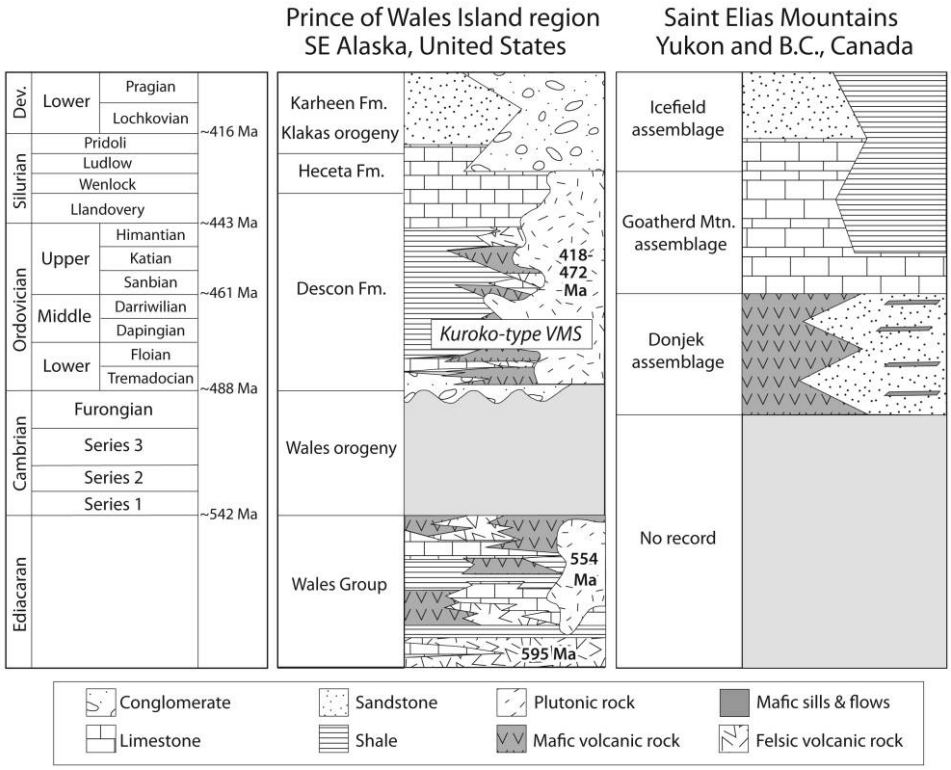

Figure 3. Ediacaran to Devonian stratigraphy of the Craig subterrane, southeastern Alaska and northwestern Canada, compiled from Gehrels and Saleeby (1987*a*), Dodds and Campbell (1992), and Mihalynuk et al. (1993). B.C. = British Columbia; Dev. = Devonian; Fm. = Formation; VMS = volcanogenic massive sulfide deposits. Geological timescale of Gradstein et al. (2004).

siliceous siltstone, graywacke, and basalt assigned to the Cannery Formation (Karl et al. 2010).

Volcanism and Sedimentation in the Saint Elias Mountains

As currently understood, the Craig subterrane in the Saint Elias Mountains (fig. 2) is composed of three Paleozoic- to early Mesozoic-age lithological units provisionally referred to as the Donjek, Goatherd Mountain, and Icefield assemblages (Gordey and Makepeace 2003; Israel 2004). A detailed history of these assemblages has been difficult to unravel because of deformation and metamorphism associated with (1) the mid-Mesozoic accretion of the Alexander terrane (McClelland and Gehrels 1990), (2) the convergence of the Yakutat microplate with the Aleutian trench (Pavlis et al. 2004), and (3) displacement along the Duke River and Denali fault systems (Cobbett et al. 2010). Cenozoic uplift has driven the Saint Elias Mountains to be one of the most inaccessible mountain ranges in North America, with topography cresting at 5900 m and extensive glacial networks that comprise the largest nonpolar icefield system on Earth.

Upper Cambrian to Middle Ordovician Donjek Assemblage. The >2000-m-thick Donjek assemblage, the focus of this study, is the oldest recognized component of the Craig subterrane in southwestern Yukon and northwestern British Columbia (figs. 3, 4). Along the length of the Saint Elias Mountains, it is mostly characterized by fine-grained, thinly to thickly bedded, planar laminated to ripple cross-laminated, quartzose to calcareous siltstone and sandstone (Dodds and Campbell 1992). Concordant 0.5–12-m-thick mafic sills and pillowed to massive basalts interbedded with the sandstone sequences locally constitute up to 80% of the section over intervals of hundreds of meters (Mihalynuk et al. 1993). A shallow-marine depositional environment is most consistent with the sedimentary and volcanic rock types and observed sedimentary structures (Mihalynuk et al. 1993). Quartz-rich sandstone units likely indicate a continental source region adjacent to the Craig subterrane. Depositional-age constraints are limited to poorly preserved Late Cambrian to Early Ordovician cono-

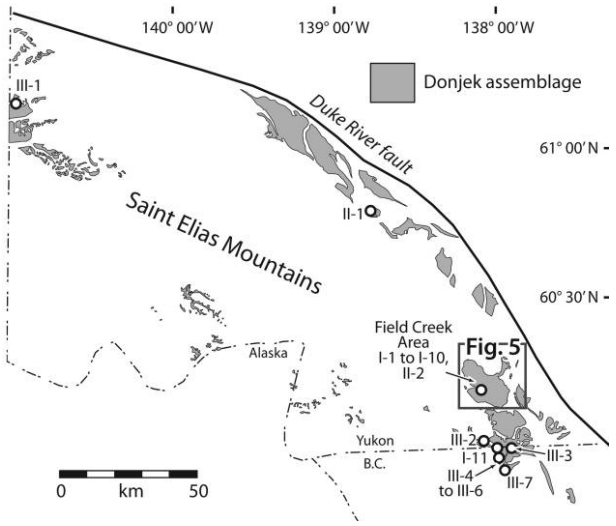

Figure 4. Map distribution of Upper Cambrian to Middle Ordovician mafic volcanic and sedimentary rocks of the Donjek assemblage in the Saint Elias Mountains of Yukon and northwestern British Columbia (after Dodds and Campbell 1992). Outcrop patterns are largely the result of modern structural trends and cover by glacial ice. The circles indicate the locations of geochemical samples obtained from the Donjek assemblage.

donts and bivalves (Dodds et al. 1993). The Donjek assemblage is conformably overlain by limestone that yields Early to Middle Ordovician conodont (*Drepanoistodus* sp., *Variabiloconus basslieri* Furnish), cephalopod (ellesmeroceroid), and gastropod (*Pararaphistoma* sp.) fauna (Dodds et al. 1993).

The Field Creek volcanics are a well-exposed succession of Donjek assemblage strata in the Field Creek area of southwestern Yukon (Dodds and Campbell 1992; fig. 4). In this region, volcanic and volcaniclastic rocks crop out along the limbs of the Bates River antiform (fig. 5). Feldspathic sandstone in this succession yields Late Cambrian to Early Ordovician brachiopods *Billingsella* sp. and *Ocnerorthis* sp. (Dodds et al. 1993). The Field Creek volcanics are overlain by Early to Middle Ordovician carbonate rocks (Dodds et al. 1993).

Ordovician to Silurian Goatherd Mountain Assemblage. The Ordovician to Silurian Goatherd Mountain assemblage primarily consists of thickly bedded to massive limestone, limestone conglomerate, argillite, and calcareous sandstone (Dodds and Campbell 1992; Mihalynuk et al. 1993; fig. 3). Most units are recrystallized and foliated. Bedding is typically transposed, and many Goatherd Mountain assemblage rocks in northwestern British Columbia are deformed into a complex array of ptygmatic folds (Mihalynuk et al. 1993). A shallow-marine depositional environment is inferred for the thickly bedded to massive limestone (Dodds and Campbell 1992; Mihalynuk et al. 1993). Deepwater or slope environments are indicated by calcareous turbidites that locally preserve complete Bouma sequences (with divisions A, B, C ± D, and E; A, B, C or distal C, D, E; and A, E; Mihalynuk et al. 1993). The turbiditic rocks grade laterally into argillite units that yield Middle to Late Ordovician graptolites of the *Pseudoclimacograptus decoratus* and *Climacograptus bicornis* zones (Norford and Mihalynuk 1994). These argillite units host massive, clast-supported limestone conglomerates that probably represent debris flow deposits generated by tectonic instability, oversteepening of the adjacent platform margin, or the migration of facies boundaries (Mihalynuk et al. 1993).

Devonian to Triassic Icefield Assemblage. Mid-Paleozoic to early Mesozoic strata of the Saint Elias Mountains are assigned to the Icefield assemblage. In northwestern British Columbia, Devonian (and Silurian?) rocks mostly include red-brown to orange weathering, medium to thickly bedded to massive, planar cross-stratified, lithic sandstone to polymictic conglomerate (Mihalynuk et al. 1993; fig. 3). Lithic fragments in the sandstone and conglomerate consist of chert, argillite, and volcanic rocks. Fern fronds and other plant fossils occur in some of the sandstone units (Mihalynuk et al. 1993). Black argillite and limestone are locally interbedded with the coarse siliciclastic rocks. These features suggest that at least some Icefield assemblage strata were deposited in a terrigenous to shallow-marine setting, similar to units of the Karheen Formation in southeastern Alaska (Mihalynuk et al. 1993).

Principal Lithofacies of the Field Creek Volcanics

New field studies were performed in the Field Creek area of southwestern Yukon to identify the depositional setting and emplacement processes of the Field Creek volcanics. Our efforts focused on delineating the associations of primary and resedimented volcanic and marine sedimentary lithofacies, since facies analysis is useful to constrain volcanic processes and environments in a variety of tectonic settings (e.g., McPhie and Allen 1992; McPhie 1995; Busby and Bassett 2007).

We measured and studied a 900-m-thick succession along a single transect from the core to the southern limb of the Bates River antiform (figs. 5, 6) and observed three principal facies associations (table A1, available in the online edition or from the

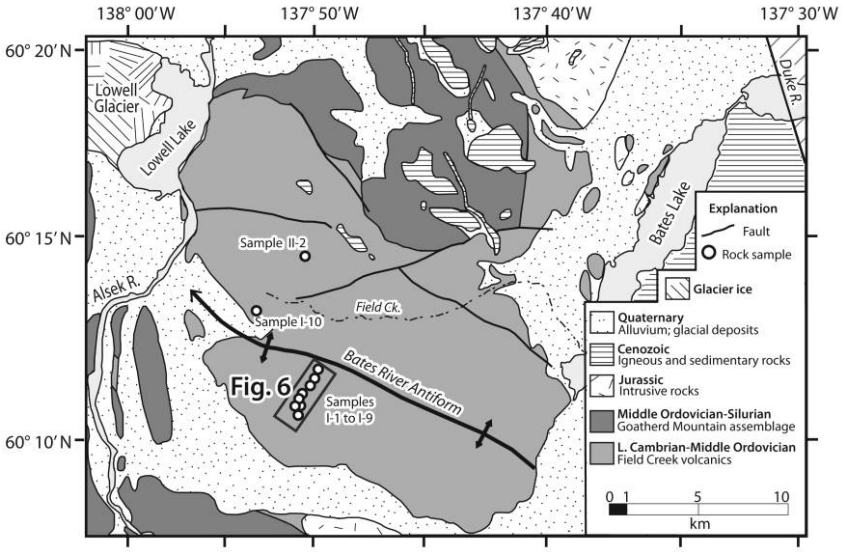

Figure 5. Simplified geological map of the Bates River antiform, Saint Elias Mountains, southwestern Yukon (after Dodds and Campbell 1992). Circles indicate the locations of geochemical samples discussed in the text. The box indicates the location of the stratigraphic section of figure 6. Ck. = creek; R. = river.

Journal of Geology office; fig. 6). The basaltic facies association comprises facies related to the eruption of primary volcanic products. It includes coherent lavas (massive and pillow basalt; fig. 7*A*, 7*B*) and fluidal to blocky peperite (sediment-matrix basalt breccia; fig. 7*C*, 7*D*). The volcanogenic sedimentary facies association consists of three facies primarily formed by the reworking of units from the basaltic facies association. Planar laminated and planar to trough cross-stratified sandstone and polymictic pebble conglomerate (fig. 8*A*) represent most rock types of the volcanogenic sedimentary facies association. Minor components include in situ to partly to wholly resedimented hyaloclastite (monomictic basalt breccia; fig. 8*B*) and massive, polymictic cobble to boulder conglomerate (fig. 8*C*). The limestone-sandstone facies association is composed of silty limestone and fossiliferous sandstone.

Carbonate facies and sedimentary structures that form under high-energy conditions indicate a shallow-marine environment for the Field Creek volcanics. Pillow lavas, hyaloclastite, and peperite also corroborate the interpretation of a subaqueous depositional environment. Similar facies associations have been documented in modern back-arc settings, such as the Lau (e.g., Hawkins 1995) and Shikoku (e.g., Kobayashi et al. 1995) basins. Shallow submarine volcanic settings, such as submerged arc fronts, locally contain similar successions; however, arc-front stratigraphy is expected to contain pumiceous facies from explosive eruptions.

Lithogeochemistry

Twenty samples of the Donjek assemblage were selected for major- and trace-element geochemistry. Rock samples prefaced by 09VL, 09VLB, and 10VLB collection numbers (table A2, available in the online edition or from the *Journal of Geology* office) were analyzed with inductively coupled plasma–mass spectrometry (ICP-MS) at Activation Laboratories in Ancaster, Ontario. Samples prefaced by MMI and MSM (table A2) were analyzed by ICP-MS and x-ray fluorescence at Memorial University of Newfoundland and the Cominco Exploration Research Laboratory in Vancouver, British Columbia, respectively.

Petrographic examination indicated that the rock samples have been affected by low-grade prehnite-pumpellyite to greenschist facies metamorphism. Some major (Na, K, Ca) and low-field-strength (Cs, Rb, Ba, Sr, U) elements are mobile under these low-grade conditions (e.g., MacLean and Barrett 1993). The following geochemical results and discussions are based mostly on high-field-strength elements (HFSEs: Hf, Nb, Ta, Y, Zr, Sc), rare earth elements (REEs), transition elements (V, Cr, Ni, Co), major elements (Ti, Al), and Th, all thought to be immobile during alteration and metamorphism (e.g., Pearce and Cann 1973; Wood 1980; Jenner 1996).

Geochemical Characteristics. Most Donjek assemblage volcanic rocks have lithological and textural characteristics that make them generally in-

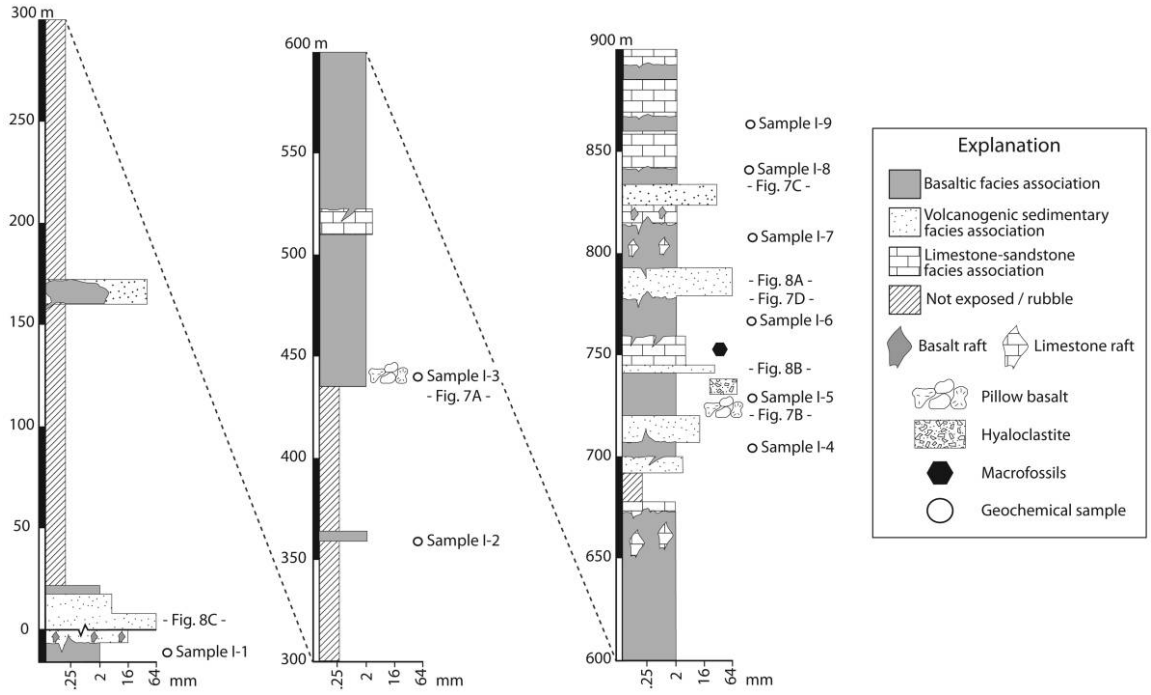

Figure 6. Generalized stratigraphic section of the Field Creek volcanics, showing the distribution of units that constitute the basaltic, volcanogenic sedimentary, and limestone-sandstone facies associations along the southern limb of the Bates River antiform. The approximate locations of geochemical samples and photo stations mentioned in the text (figs. 7, 8) are shown adjacent to the stratigraphic columns.

distinguishable in the field. Despite this, they can be subdivided into three compositionally distinct types.

Type I rocks (n = 11) represent 10 volcanic flows and a synvolcanic dike from southwestern Yukon and northwestern British Columbia, mostly within the Field Creek volcanics (samples I-1–I-11; figs. 4–6). They are classified as subalkalic basalts on the basis of their Zr/TiO_2 and Nb/Y ratios (fig. 9). Basaltic and subalkalic affinities are also consistent with SiO_2 values of 46–51 wt% (fig. 10*A*).

Moderate to high degrees of crystal fractionation are expressed by Mg#'s that vary from 36 to 61, signifying that type I basalts do not represent primary mantle melts. A tholeiitic differentiation trend is indicated by smoothly increasing TiO_2, Fe_2O_3, Nb, Sm, and Yb contents with increasing fractionation, as monitored by Mg# and Zr (fig. 10*B*, 10*C*, 10*F*–10*H*); decreasing Al_2O_3 and Ni contents with increasing fractionation are also supportive of a tholeiitic differentiation trend (fig. 10*D*, 10*E*).

Type I basalts have negative sloping primitive mantle–normalized multielement patterns (fig. 11*A*) with moderate light-REE enrichment (La/Sm_{PM} = 1.5–2.0, where PM is for normalized to primitive mantle of Sun and McDonough 1989), weakly negative Nb anomalies with respect to Th (Nb/Th_{PM} = 0.5–0.9), positive Zr anomalies, and relatively flat heavy-REE patterns (Sm/Yb_{PM} = 1.6–2.0). Most samples display negative to positive Eu and Ti anomalies that are probably linked to the fractionation and/or accumulation of plagioclase and Fe-Ti oxide minerals.

Type II rocks (n = 2) comprise a massive flow from the central Saint Elias Mountains of southwestern Yukon and a domelike mound in the northern limb of the Bates River antiform (samples II-1, II-2; figs. 4, 5). These rocks are categorized as subalkalic basalts that yield Nb/Y and Zr/TiO_2 ratios distinct from those in other rock samples of the Donjek assemblage (fig. 9). Type II rocks have some of the highest SiO_2 values (50 and 55 wt% for samples II-1 and II-2, respectively) in the sample suite (fig. 10*A*). The values for TiO_2 (0.95 and 2.1 wt%), Fe_2O_3 (8 and 14 wt%), and MgO (2.2 and 3.2 wt%) are generally lower than those of type I basalts (table A2). Relatively high degrees of crystal fractionation are evidenced by Mg#'s of 22 and 44 and Ni, Cr, and Co contents typically <20 ppm. A tholeiitic differentiation trend is suggested by increasing

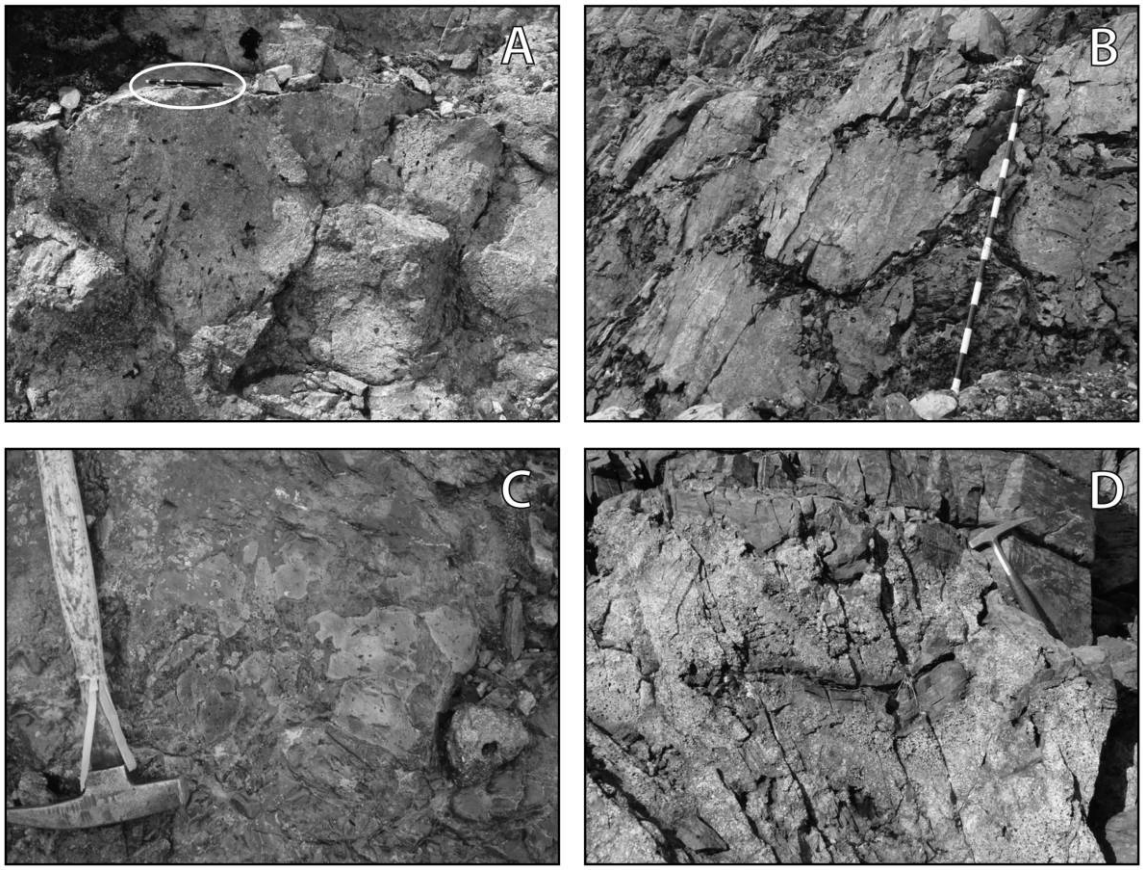

Figure 7. Representative rock types of the basaltic facies association in the Field Creek volcanics; photos taken along the stratigraphic section illustrated in figure 6. *A*, Vesicular pillow basalt porphyry sampled at 440 m (sample I-3); pencil for scale (circled). *B*, Vesicular pillow basalt sampled at 730 m (sample I-5); jacob staff for scale: each bar represents 10 cm. *C*, Fluidal peperite texture consisting of amoeboid-shaped, lapilli- to block-sized basalt fragments in brown to purple volcaniclastic sand matrix at 840 m; rock hammer for scale. *D*, Undulatory and intermingled contact between massive feldspar porphyry lava and overlying well-bedded, fossiliferous sandstone at 780 m. The contact is characterized by rafts of laminated sandstone within locally highly vesicular ("frothy"), coherent lava, defining peperite texture, and it indicates intrusion into wet sediment; rock hammer for scale.

TiO_2, Fe_2O_3, Nb, Sm, and Yb contents, with fractionation as monitored by Mg# and Zr (fig. 10*B*, 10*C*, 10*F*–10*H*).

Type II rocks are distinguished by their negative sloping primitive mantle–normalized multielement patterns, with moderately to strongly negative Nb (Nb/Th_{PM} = 0.19 and 0.61) and Ti anomalies (fig. 11*B*). The light-REE (La/Sm_{PM} = 1.4 and 2.7) and heavy-REE (Sm/Yb_{PM} = 2.0 and 3.3) patterns are more enriched than those of type I basalts.

Type III rocks (n = 7) consist of volcanic flows and sills from western Yukon and northwestern British Columbia (samples III-1–III-7; fig. 4). Although their Zr/TiO_2 ratios overlap those of type I and II basalts, some type III rocks have significantly higher Nb/Y ratios (0.63) that suggest affinities with alkali basalt (fig. 9). Type III rocks have major-element signatures generally similar to those of type I basalts, including high TiO_2 (1.7–3.1 wt%) and moderate Al_2O_3 (13–17 wt%), Fe_2O_3 (10–14 wt%), and MgO (3.8–7.6 wt%) contents (table A2).

Moderate degrees of crystal fractionation are illustrated by Mg#'s that vary from 41 to 57. The observed compatible- and incompatible-element contents are consistent with tholeiitic differentiation trends, such as increasing TiO_2, Fe_2O_3, Nb, Sm, and Yb with progressive fractionation. These differentiation trends have slopes that are similar to those of type I basalts (fig. 10*B*, 10*C*, 10*F*–10*H*).

Type III rocks consistently show positive Nb anomalies relative to Th (Nb/Th_{PM} = 1.1–1.5) in primitive mantle–normalized multielement dia-

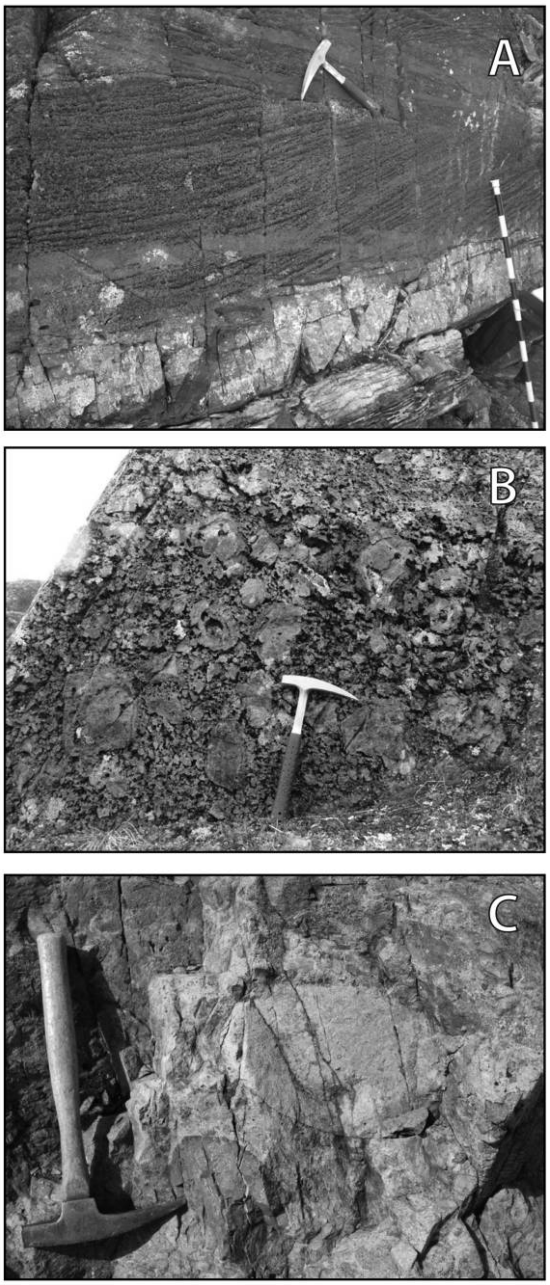

Figure 8. Representative rock types of the volcanogenic sedimentary facies association in the Field Creek volcanics. Photos taken along the measured stratigraphic section illustrated in figure 6. *A*, Well-stratified sandstone to pebble conglomerate at 790 m; jacob staff for scale: each bar represents 10 cm. Large-scale (0.40-m) planar cross-beds of well-sorted conglomerate overlie planar laminated, medium- to coarse-grained sandstone. *B*, In situ to partly resedimented hyaloclastite at 745 m associated with underlying pillow basalt at 730 m; rock hammer for scale. *C*, Massive, polymictic boulder conglomerate at base of the measured section, directly overlying sample I-1; rock hammer for scale.

grams (fig. 11*C*). The samples exhibit light-REE patterns (La/Sm_{PM} = 1.0–2.1) similar to those of type I and II basalts but have higher heavy-REE ratios (Sm/Yb_{PM} = 1.8–3.7; fig. 11*C*).

Neodymium Isotope Geochemistry

Nd isotope geochemistry is a valuable tool for characterizing the relative contributions of crust and mantle involved in magmatism, because the Sm-Nd isotopic system is very resistant to alteration, metamorphism, and fractionation (DePaolo 1988). The Nd isotopic compositions were measured for five Donjek assemblage samples (table A3, available in the online edition or from the *Journal of Geology* office). They were analyzed with isotope dilution and thermal ionization mass spectrometry at the Isotope Geochemistry and Geochronology Research Centre at Carleton University in Ottawa, Ontario. Nd isotope data are presented relative to an in-house standard equivalent to the $^{143}Nd/^{144}Nd = 0.511849 \pm 0.000011$ (2σ) value for the La Jolla standard.

Initial ε_{Nd} values for the rock samples were calculated at the Cambrian-Ordovician boundary (488 Ma) in the timescale of Gradstein et al. (2004). At this time, ε_{Nd} values for depleted mantle range from +7.2 (DePaolo 1981) to +8.8 (Goldstein et al. 1984). Each of the five samples yielded $\varepsilon_{Nd(488\,Ma)} > 0$ (i.e., greater than CHUR [chondritic uniform reservoir]) and less than that of depleted mantle. Type I and II rocks with weakly to strongly negative Nb anomalies have $\varepsilon_{Nd(488\,Ma)}$ = +5.2 and +4.6. Type III rocks

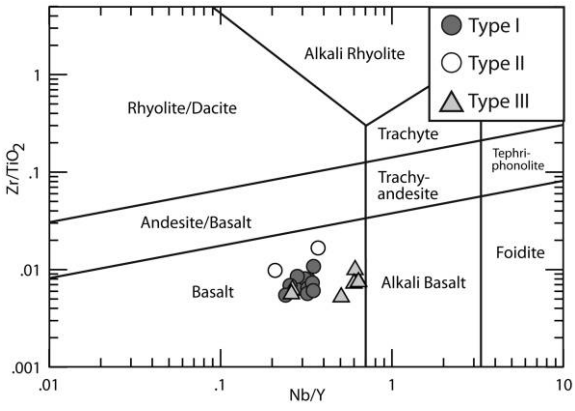

Figure 9. Zr/TiO_2-Nb/Y diagram of Winchester and Floyd (1977), as modified by Pearce (1996), showing the lithological classification of the Donjek assemblage rock samples.

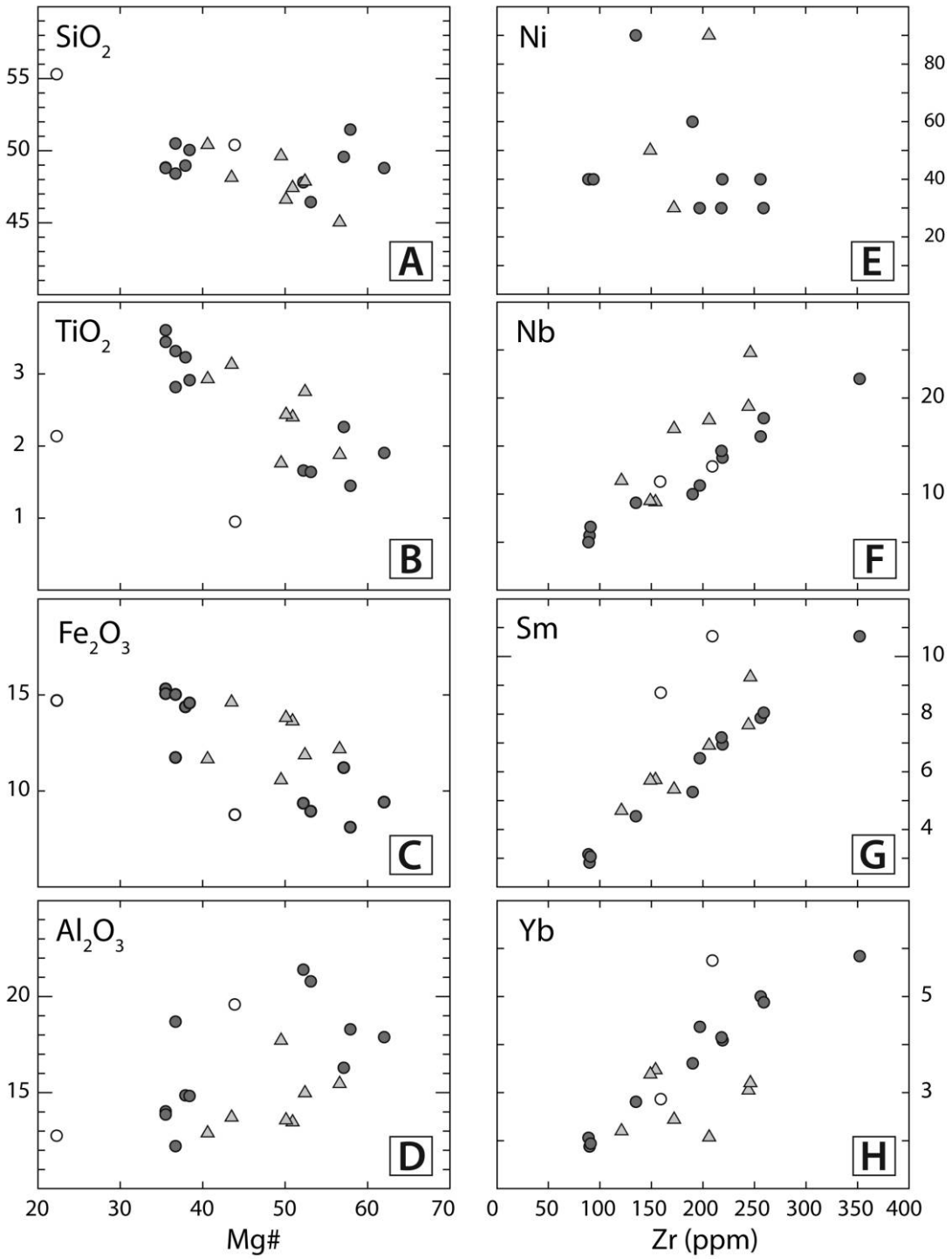

Figure 10. Major- and trace-element variation diagrams for the Donjek assemblage samples. SiO_2 (*A*), TiO_2 (*B*), Fe_2O_3 (*C*), and Al_2O_3 (*D*) versus Mg#; Ni (*E*), Nb (*F*), Sm (*G*), and Yb (*H*) versus Zr. Symbols are as in figure 9.

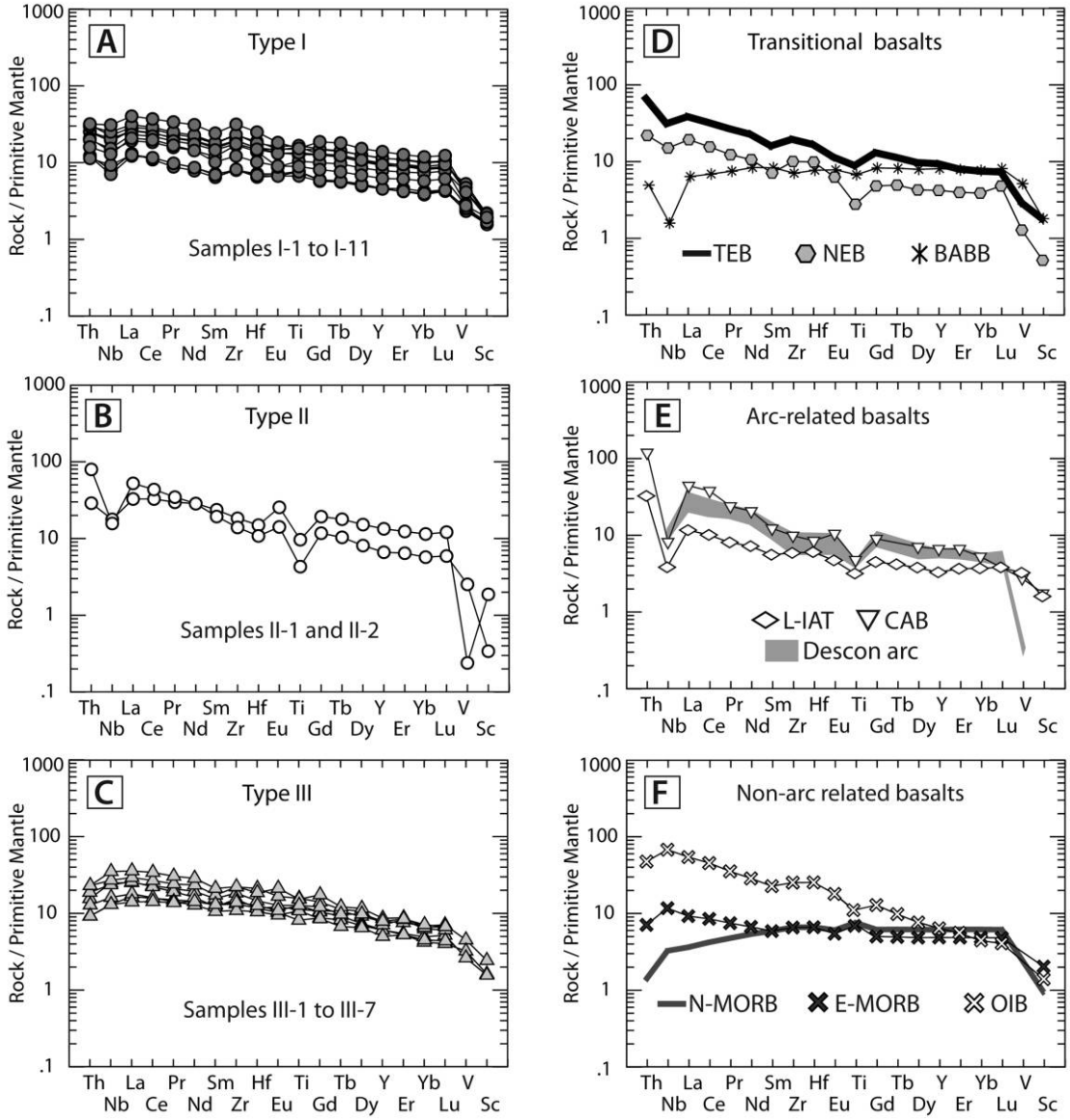

Figure 11. Primitive mantle–normalized multielement plots of rocks from the Donjek assemblage and global magmatic systems. *A*, Type I basalts. *B*, Type II basalts. *C*, Type III basalts. *D*, Transitional basalts: Th-enriched (TEB), Nb-enriched (NEB), and back-arc basin basalts (BABB) of Piercey et al. (2004). *E*, Arc-related basalts: light rare earth element–enriched island-arc tholeiite (L-IAT) of Shinjo et al. (2000), calc-alkaline basalt (CAB) of Stolz et al. (1990), and Descon arc (Gehrels and Saleeby 1987*b*). *F*, Non-arc-related basalts: normal and enriched mid-ocean ridge basalt (N-MORB and E-MORB, respectively) and ocean-island basalt (OIB; Sun and McDonough 1989). Primitive-mantle normalizing values are from Sun and McDonough (1989) and McDonough and Sun (1995).

with positive Nb anomalies yield $\varepsilon_{Nd(488\,Ma)} = +3.7$ to +5.8.

Discussion

Evidence for Arc and Nonarc Geochemical Affinities. The geochemical signatures of the Donjek assemblage samples indicate that magmas of at least three different compositions were associated with Late Cambrian to Middle Ordovician volcanic systems in the Saint Elias Mountains. Tectonic-discrimination diagrams such as those in figure 12 provide the broadest insight into the setting of this magmatism, including trace-element characteristics that fingerprint arclike or non-arclike volcanism. In the Nb-Hf-Ta ternary diagram of Wood (1980), so-called transitional signatures that informally refer to both arclike and non-arclike com-

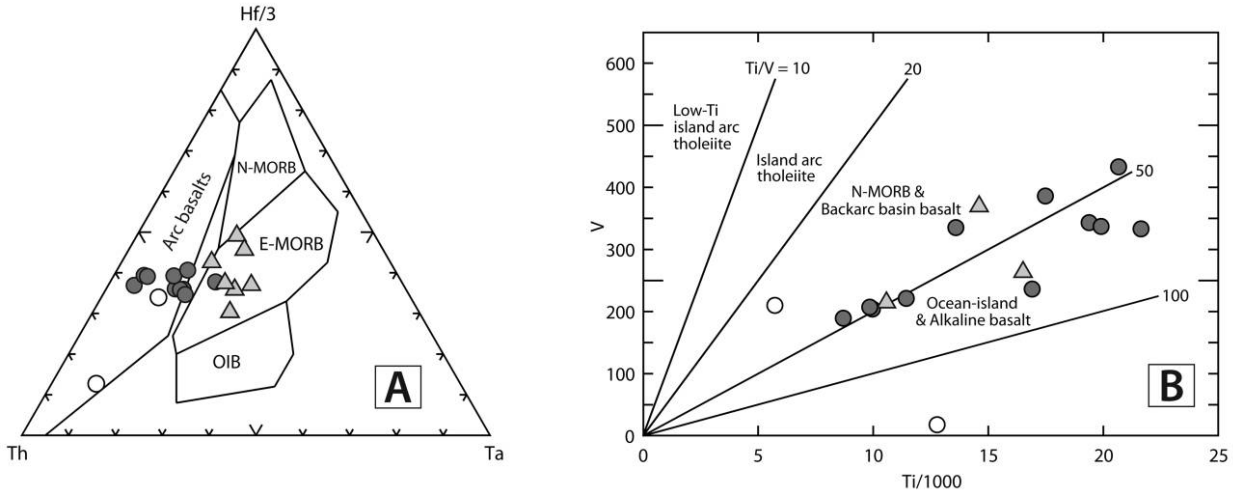

Figure 12. Tectonic discrimination diagrams for the Donjek assemblage rocks. *A*, Th-Nb-Ta diagram of Wood (1980). *B*, Ti-V diagram of Shervais (1982). Symbols are as in figure 9. E-MORB = enriched mid-ocean ridge basalt; N-MORB = normal mid-ocean ridge basalt; OIB = ocean-island basalt.

positions are displayed by type I samples, which plot in the fields for volcanic-arc basalt and enriched mid-ocean ridge basalt (E-MORB; fig. 12*A*). Type II samples enriched in light REEs and strongly depleted in Nb and Ti show geochemical similarities with volcanic-arc basalts, whereas type III samples plot within the E-MORB field (fig. 12*A*). In the Ti-V plot of Shervais (1982), most Donjek samples show transitional signatures (Ti/V = 45–70) and plot in the compositional fields defined for normal mid-ocean-ridge basalt (N-MORB), back-arc basin basalt (BABB), ocean-island basalt (OIB), and alkaline basalt (fig. 12*B*).

A robust indication of the tectonic setting is observed by comparing the primitive mantle–normalized trace-element contents with those of modern volcanic systems (fig. 11). The transitional geochemical affinities of type I basalts resemble Th-enriched, Nb-enriched, and back-arc basin lavas (fig. 11*D*) that form by decompressional melting of subarc mantle during intra-arc rifting (e.g., Kepezhinskas et al. 1997; Shinjo et al. 2000; Piercey et al. 2004; Escuder Viruete et al. 2007). The negative Nb anomalies ($Nb/Th_{PM} < 0$) and light-REE enrichment of these transitional basalts (fig. 11*D*) reflect the diagnostic "arc signature" typical of magmas from mantle sources with a subduction-related component or contamination from crustal material (e.g., Arculus and Powell 1986; Pearce and Peate 1995). The subduction-related component probably results from the dehydration of silicate minerals within the descending slab, leading to the transfer of mobile elements such as Th into the subarc mantle wedge. The retention of HFSEs in accessory minerals within the slab produces HFSE depletion in arc magmas, particularly for Nb.

Type II rocks have the enriched light-REE patterns and negative Nb and Ti anomalies of volcanic-arc basalts (fig. 11*E*) such as light-REE–enriched island-arc tholeiite from the Ryukyu arc of Japan (Shinjo et al. 2000) and calc-alkaline basalt from the Sunda arc of Indonesia (Stolz et al. 1990). Mafic to intermediate volcanic and intrusive rocks of the Descon arc analyzed by Gehrels and Saleeby (1987*b*) display light-REE and HFSE signatures that compare favorably with those of our type II basalts (fig. 11*E*).

Type III basalts uniformly show positive Nb anomalies ($Nb/Th_{PM} > 0$) that are the hallmark of non-arc-related magmatic rocks (fig. 11*F*). The light-REE enrichment and relatively high HFSE contents of the type III basalts are most similar to E-MORB and OIB lavas that occur in continental-margin and arc rifts and continental flood basalt provinces (e.g., Sun and McDonough 1989; Piercey et al. 2006).

Mantle and Slab Contributions. The mantle sources involved in the generation of basalts are best discriminated with incompatible and immobile trace elements that are not greatly influenced by crustal contamination, slab metasomatism, or fractionation processes. As described by Pearce and Peate (1995), Zr/Yb and Nb/Yb ratios are particularly useful for discerning mantle signatures in arc systems. In a Zr/Yb-versus-Nb/Yb plot (fig. 13), the Donjek assemblage samples form a linear trend ex-

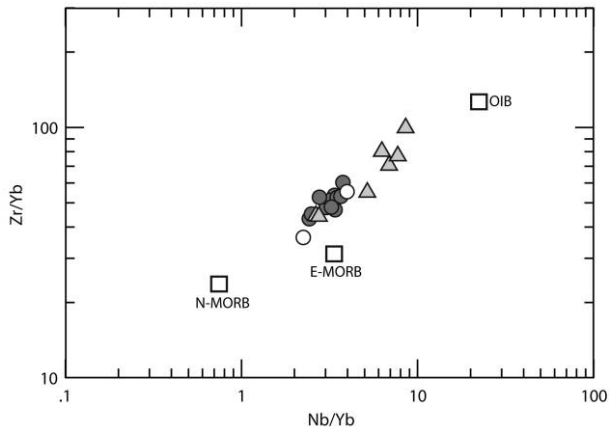

Figure 13. Zr/Yb-versus-Nb/Yb diagram (after Pearce and Peate 1995). Average values of normal mid-ocean ridge basalt (N-MORB), enriched mid-ocean ridge basalt (E-MORB), and ocean-island basalt (OIB) reservoirs from Sun and McDonough (1989). Symbols are as in figure 9.

tending from the global average of E-MORB toward that of OIB. The Zr and Nb concentrations and E-MORB-like characteristics of type I and II rocks are generally consistent with arc basalts, whereas the more significant Zr and Nb concentrations and OIB-like characteristics of type III rocks are in agreement with non-arclike basalts. Overall, the geochemical signatures for the three rock types indicate mantle sources that are moderately to strongly incompatible-element enriched.

Subcontinental-mantle lithosphere and enriched (undepleted) asthenospheric mantle are the most likely sources for E-MORB- and OIB-like signatures in arc systems. Mafic rocks derived from the partial melting of subcontinental-mantle lithosphere are strongly enriched in incompatible elements and relatively depleted in Nb and Ti and yield initial ε_{Nd} values that typically range from −20 to +5 (e.g., Allègre et al. 1982; Rogers and Hawkesworth 1989; Hawkesworth et al. 1990). The geochemical characteristics of subcontinental-mantle lithosphere are probably the result of enrichment from subduction-related processes. The partial melting of enriched asthenospheric mantle is interpreted to produce mafic rocks with variable Nb/Th signatures and initial ε_{Nd} values that range from 0 to +9 (e.g., Hochstaedter et al. 1990; Gorring and Kay 2001; Kuzmichev et al. 2005). Geochemical contributions from enriched asthenosphere typically occur as upwelling mantle is injected beneath extensional-arc systems (e.g., van Staal et al. 1991; Shinjo et al. 1999). In a hybrid model, upwelling N-MORB-type asthenosphere may mix with subducted sediment or subcontinental-mantle lithosphere to generate enriched lava compositions in extensional-arc systems (e.g., Pouclet et al. 1995; Piercey et al. 2004).

In light of these data, the geochemical signatures of the Donjek assemblage basalts are most compatible with enriched asthenospheric mantle sources. In a Th/Yb-versus-Nb/Yb diagram (fig. 14), type I and II basalts show Th enrichment (high Th/Yb for a given Nb/Yb) not characteristic of magmatic rocks that define the nonarc mantle array. This Th enrichment probably reflects a true "arc signature," as the Nd isotopic compositions of these rocks are generally inconsistent with subcontinental-mantle lithosphere or contamination from crustal material. For example, the relatively high initial ε_{Nd} values of type I and II basalts (+4.6 and +5.2, respectively) are intermediate to the values for CHUR and the depleted-mantle curve, illustrating that there was little to no contribution from Proterozoic crustal rocks (fig. 15). Ordovician rocks of the Descon arc yield initial ε_{Nd} values (+3.3 to +4.6) that also support mantle sources with limited contamination from crustal material (Samson et al. 1989). In contrast, type III basalts lack Th enrichment in Th/Yb-versus-Nb/Yb space and plot within the nonarc mantle array, mostly near the global average for E-MORB (fig. 14). Because the initial ε_{Nd} values of type III basalts (+3.7 to +5.8) overlap those of type I and II rocks (fig. 15), it seems likely that most or all of the Donjek assemblage samples can be modeled by using a common E-MORB to OIB-like asthenospheric mantle source.

Although the origins of enriched reservoirs in the upper mantle continue to be debated (e.g., Fitton

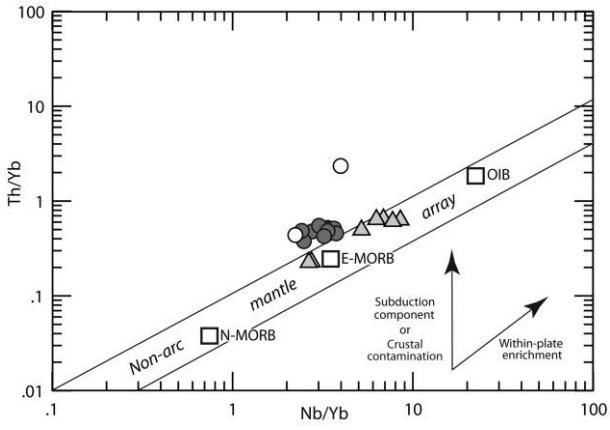

Figure 14. Th/Yb-versus-Nb/Yb diagram (after Pearce and Peate 1995). Average values of normal mid-ocean ridge basalt (N-MORB), enriched mid-ocean ridge basalt (E-MORB), and ocean-island basalt (OIB) reservoirs from Sun and McDonough (1989). Symbols are as in figure 9.

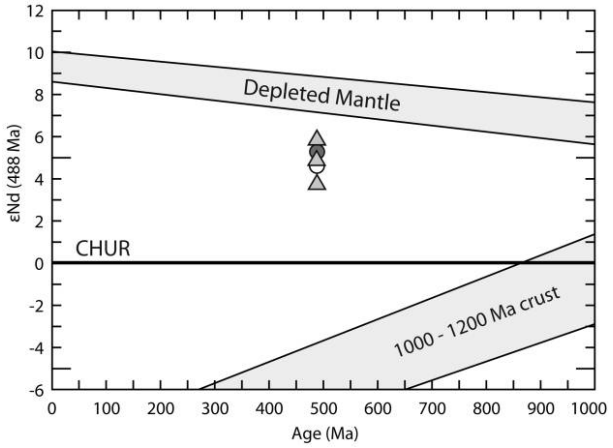

Figure 15. ε_{Nd} versus age for samples of the Donjek assemblage. Depleted mantle curve: lower limit from DePaolo (1981), upper limit from Goldstein et al. (1984). Proterozoic crustal curve from Samson et al. (1995). Symbols are as in figure 9. CHUR = chondrite uniform reservoir (Bulk Earth).

2007), prior studies of arc systems have assumed similar E-MORB- to OIB-like sources to have variable light-REE enrichment ($^{147}Sm/^{144}Nd$ = 0.18–0.20) and moderately positive $\varepsilon_{Nd(t)}$ values (+3 to +7; e.g., Swinden et al. 1990). Using these geochemical constraints, we illustrate possible mixing and partial melting relationships for the Donjek assemblage basalts in an $\varepsilon_{Nd(t)}$-versus-$^{147}Sm/^{144}Nd$ diagram (fig. 16). The incompatible-element contents and Nd isotopic compositions of type I basalts can be generally modeled as a 4%–10% partial melt of an OIB-like mantle source that either contains or was mixed with a subduction-related component. Type II basalt compositions are likely produced by 1%–4% partial melting of an OIB-like asthenospheric mantle source that was mixed with a subduction-related component, with substantial subsequent fractional crystallization. Rocks of the Descon arc analyzed by Samson et al. (1989) display geochemical characteristics and partial-melting relationships strikingly similar to those in type II basalts (DA field in fig. 16). Type III basalts probably represent a 7%–10% partial melt of an OIB-like source that had not been impregnated by or mixed with subduction-related components. Various proportions of a depleted-mantle source can be accommodated in the partial-melting models for each of the Donjek assemblage rock types.

Tectonic Setting and Modern Analogues. Direct comparisons with volcanic rocks in modern arc systems are essential for evaluating the plate tectonic setting of the Donjek assemblage. Mafic rocks that erupt during the rifting of volcanic arcs and formation of back-arc basins are interpreted to most closely match the enriched-mantle compositions and geochemical signatures of the Donjek assemblage. We propose that mafic rocks of Izu-Ogasawara arc–Sumisu Rift and Ryukyu arc–Okinawa Trough in the western Pacific Ocean are representative modern analogues.

The Sumisu Rift occurs within the actively rifting Izu-Ogasawara arc. Subaqueous volcanic rocks in the Sumisu Rift are located near cross-arc structures and not localized along an axial rift or spreading center (Taylor et al. 1990). The Sr-Nd-Pb isotopic compositions and trace-element signatures of mafic lavas in the Sumisu Rift resemble E-MORB with a moderate subduction component, whereas adjacent Izu-Ogasawara arc-front lavas have a more-depleted source with a strong subduction component (Hochstaedter et al. 1990). Mantle upwelling and injection of enriched asthenospheric material beneath the Sumisu Rift may explain the E-MORB source (Hochstaedter et al. 1990). Hydrothermal circulation systems in the Sumisu Rift have led to the exhalation of VMS deposits that may be a modern analogue for the Kuroko district (Taylor et al. 1990).

The Okinawa Trough is a young back-arc basin that formed by extension of Asian continental lithosphere behind the Ryukyu arc system from southern Japan to Taiwan. Quaternary basalts in the Okinawa Trough possess isotopic and trace-element compositions that imply sources from E-MORB- to OIB-like asthenospheric mantle and a subduction

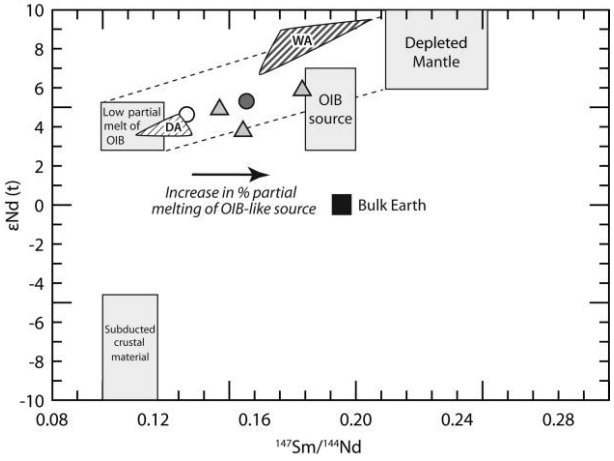

Figure 16. An ε_{Nd}-versus-$^{147}Sm/^{144}Nd$ diagram (after Swinden et al. 1990) illustrating possible partial melting and mixing relationships for the Donjek assemblage basalts. See text for discussion OIB = ocean-island basalt. Descon arc (DA) and Wales arc (WA) samples from Samson et al. (1989). Symbols are as in figure 9.

component (Shinjo et al. 1999). Rifting in the southern Okinawa Trough may have been dynamically linked to the onset of north-directed subduction and related extension with the Ryukyu arc after collisional tectonics in Taiwan. For example, postcollisional extension in northern Taiwan led to asthenospheric upwelling and eruption of mafic lavas with enriched-mantle affinities (Wang et al. 1999, 2002).

There is evidence that the tectonics of the Wales orogeny have affected the nature of younger magmatism on the Alexander terrane. Late Neoproterozoic rocks of the Wales arc that formed before orogeny exhibit $\varepsilon_{Nd(t)}$ and $^{147}Sm/^{144}Nd$ signatures that are consistent with depleted-mantle sources (Samson et al. 1989; WA field in fig. 16). In contrast, rocks of the Donjek assemblage and Descon Formation document an isotopic and elemental shift toward enriched-mantle compositions beneath most or all of the Alexander terrane (fig. 16). Because extended periods of arc magmatism bracket the timing of the Wales orogeny, this tectonothermal event may record an arc-arc or arc-continent collision that is the result of a downgoing plate introducing buoyant arc or continental crust into a subduction zone (e.g., Cloos 1993). Subduction of the Asian margin beneath the Luzon arc in Taiwan is an example of arc-continent collision (e.g., Huang et al. 2006), and the geochemical evidence for postcollisional upwelling of enriched mantle in the Okinawa Trough may be an appropriate analogue for the Alexander terrane in Late Cambrian to Middle Ordovician time. Another modern example of changing mantle sources related to collisional tectonics occurs where the New Hebrides arc (Vanuatu Islands) is converging with an ancient island-arc complex, referred to as the d'Entrecasteaux Zone. The collision in Vanuatu has brought enriched mantle from the back-arc region into the arc front and changed the composition of the mantle wedge (Peate et al. 1997). Although the nature of mantle dynamics beneath the Alexander terrane is unclear, collisional tectonics and/or arc rifting are consistent with the introduction of enriched mantle beneath the Descon arc system.

Implications for the Evolution of the Alexander Terrane. The combination of lithogeochemical, isotopic, and field studies on the Donjek assemblage lends new insights into the evolution of the Alexander terrane. In our tectonic model, we assume the Late Cambrian flare-up of the Descon arc to have resulted from subduction beneath the Alexander terrane after the Wales orogeny. The onset of subduction was followed by, or perhaps synchronous with, intra-arc rifting and deposition of the Donjek assemblage (fig. 17). Although the driving forces for rifting are uncertain, we propose that intra-arc extension was aided by dynamic changes associated with the renewal of subduction beneath the Alexander terrane. For example, some of the modern volcanic chains in the western Pacific Ocean are thought to be extending because of slab rollback, a term that refers to the trenchward retreat of the hinge of the subducting plate, which may cause extension in the overriding plate (Molnar and Atwater 1978). We posit that the exhalation of Kuroko-type VMS deposits in the lower Descon Formation documents at least part of this extensional-arc record in southeastern Alaska.

The geochemical results of this study suggest that rifting of the Descon arc led to the upwelling

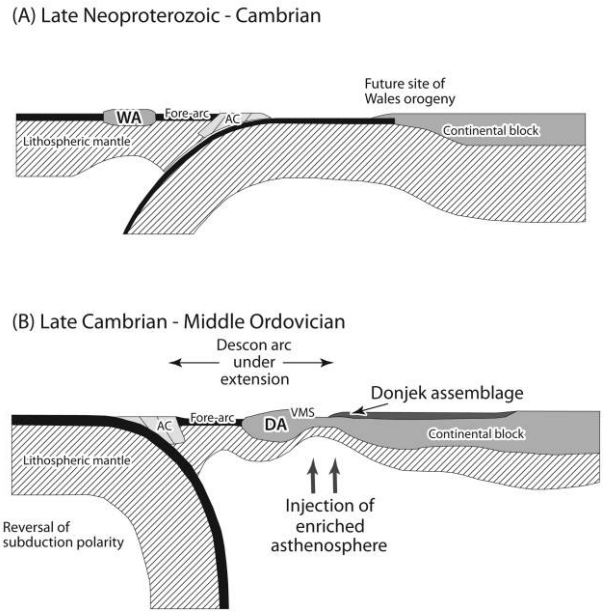

Figure 17. Schematic models showing the tectonic and magmatic evolution of the Alexander terrane, based on results from the Saint Elias Mountains. *A*, Intraoceanic subduction beneath the Wales arc during late Neoproterozoic to Cambrian time. The Wales orogeny might record the collision of the Wales arc against the edge of an adjacent continental block (Baltica?). This collision is interpreted to have caused a reversal in subduction polarity. *B*, Late Cambrian to Middle Ordovician development of the Descon arc adjacent to a continental block (Baltica?). The Descon arc is at least partially constructed on top of the remnant Wales arc. The Donjek assemblage is illustrated as being deposited a shallow-marine environment along the passive, continental side of an incipient back-arc basin. Intra-arc rifting led to the upwelling of enriched asthenosphere beneath the extending Descon arc. See text for accompanying discussion. AC = accretionary complex; DA = Descon arc; VMS = volcanogenic massive sulfide deposits of the Descon Formation in southeastern Alaska; WA = Wales arc.

and decompressional melting of enriched mantle beneath the Alexander terrane. Sequences of pebble to boulder conglomerate, cross-bedded sandstone, and pillow basalt and hyaloclastite in the Field Creek volcanics attest to an energetic marine environment with active eruptive centers. Elsewhere in the Alexander terrane, the quartzose sandstone that characterizes most of the Donjek assemblage implies stratigraphic connections to a continental block (Mihalynuk et al. 1993). We infer that the Donjek assemblage formed along the passive, continental side of an incipient back-arc basin (fig. 17), and ongoing sedimentary provenance studies are testing the possibility of a continental margin-fringing origin for the Descon arc system. This hypothesis assumes that the Wales orogeny records a late Neoproterozoic to Cambrian arc-continent (Baltica?) collisional event on the Alexander terrane, followed by a reversal of subduction polarity and formation of a continental-margin arc (Descon arc). A continental-margin setting for the Alexander terrane might also reconcile the occurrence of Precambrian detrital zircons in Karheen Formation sandstone reported by Gehrels et al. (1996).

It is unclear, however, whether rifting led to seafloor spreading and the generation of ocean crust. It is interesting to note that the Hood Bay Formation of the Admiralty subterrane contains marine sedimentary and mafic volcanic rocks whose age and character make them candidates to be considered basinal parts of the Descon back-arc region. Nonetheless, similarities between the Heceta-Goatherd Mountain and Karheen-Icefield sedimentary successions strengthen the argument that the Prince of Wales Island and Saint Elias Mountains regions were in proximity to one another in early to mid-Paleozoic time.

Implications for the Siberian-Baltican-Caledonian Lithotectonic Realm. The results from the Donjek assemblage presented here have broad implications for the development of terranes that constitute the Siberian-Baltican-Caledonian lithotectonic realm of the North American Cordillera. A number of these terranes, including the Alexander terrane, contain early Paleozoic magmatic rocks and fossil occurrences that are consistent with formation along a convergent plate-margin system in proximity to Laurentia, Baltica, and Siberia (Colpron and Nelson 2009). Our constraints on the nature of mafic magmatism and marine sedimentation in the Saint Elias Mountains allow for new correlations to be made in the western Cordillera. For example, a correlative to the Donjek assemblage is potentially recognized on the Arctic Alaska–Chukotka terrane, the microcontinental fragment that underlies most of northern Alaska and northeastern Russia. In the Seward Peninsula region of the Arctic Alaska–Chukotka terrane (fig. 1), Ordovician rocks of the Nome Group comprise a continental-platform succession that was punctuated by mafic magmatism and the exhalation of stratiform massive sulfide deposits (Till and Dumoulin 1994). Similarly to the Donjek assemblage, mafic volcanic rocks that accompanied the deposition of these platformal sequences have two affinities: (1) tholeiitic basalts with a weakly developed arc signature and (2) tholeiitic to alkalic basalts with enriched-mantle (E-MORB) compositions. Ayuso and Till (2007) considered the geochemical signatures of the Nome Group mafic rocks to record the early stages of continental, rift-related magmatism.

A growing body of geological evidence suggests that at least part of the Arctic Alaska–Chukotka terrane can be restored to the continental margin of northern Baltica in early Paleozoic time, east of the present-day trace of the northern Caledonides (Miller et al. 2010, 2011; Till et al. 2010). The Late Cambrian to Middle Ordovician history of Baltica consists of rift-related mafic magmatism and shallow-marine sedimentation associated with the development of the Uralian passive margin (Nikishin et al. 1996; Bradley 2008). Late Cambrian to Middle Ordovician arc and back-arc basin rocks of the Stekenjokk and Fundsjø sequences that are now preserved in the Scandinavian Caledonides record subduction-related magmatism along the edge of northern Baltica during the formation of this passive margin (e.g., Grenne et al. 1999). The presence of VMS deposits in the Stekenjokk and Fundsjø sequences is broadly consistent with an extensional-arc environment, and the Pb isotopic compositions of sulfide minerals therein show derivation from the mantle and Baltican crust (e.g., Bjørlykke et al. 1993).

Because the fossil, paleomagnetic, and provenance data from the Alexander terrane are consistent with latitudes near the Scandinavian Caledonides (e.g., Bazard et al. 1995), it therefore seems reasonable that the magmatic and sedimentary history of Donjek assemblage is related to that of the Nome Group and, by extension, to continental margin tectonics and arc development along northern Baltica. A speculative position for the Alexander terrane is accordingly placed near the present-day Barents and Kara sea regions of Scandinavia and Arctic Russia (AX in fig. 18). We hypothesize that the Alexander terrane was an important part of a convergent plate-margin system that included many of the terranes in the Siberian-Baltican-Caledonian lithotectonic realm (cf. Colpron and Nelson 2009). The nature of magmatism

Figure 18. Middle Ordovician paleogeographic reconstruction of the Iapetan realm of the Appalachian and Caledonian orogen and adjacent continental masses, after van Staal et al. (2011). The added position of the Alexander terrane (AX) is based on our results from the Saint Elias Mountains. The Alexander terrane is interpreted to have been proximal to other Ordovician to Silurian arc terranes of the Siberian-Caledonian-Baltican (S-B-C) lithotectonic realm (cf. Colpron and Nelson 2009) in the Barents and Kara sea areas near present-day Scandinavia and Arctic Russia. Reconstruction is largely based on a compilation of existing paleontological and paleomagnetic data presented in Cocks and Torsvik (2005, 2007) and Pisarevsky et al. (2008).

and sedimentation on these terranes, testable by future studies, may further resolve their paleogeographic and tectonic significance.

Conclusions

Upper Cambrian to Middle Ordovician mafic volcanic rocks of the Donjek assemblage in the Saint Elias Mountains have geochemical and geological attributes that are interpreted as recording the rifting of the Descon arc and the establishment of a shallow-marine back-arc basin. The volcanic rocks are subdivided into three geochemical types: transitional basalt (type I), light-REE–enriched island-arc tholeiite to calc-alkaline basalt (type II), and enriched mid-ocean ridge to ocean-island basalt (E-MORB to OIB; type III). The eruption of the volcanic rocks was likely the result of the decompressional partial melting of upwelling asthenospheric mantle beneath the incipient rift. The asthenospheric mantle was moderately to strongly incompatible-element enriched, similar to modern E-MORB and OIB. Various proportions of subduction-related and depleted-mantle sources mixed with the enriched asthenosphere to generate the range of geochemical types in the Saint Elias Mountains. The data presented in this study provide new ideas about the evolution of terranes assigned to the Siberian-Baltican-Caledonian lithotectonic realm of the North American Cordillera and provisionally place the Alexander terrane near northern Baltica in early Paleozoic time. Rift-related volcanic and sedimentary rocks of the Donjek assemblage are similar in age and character to those of the Nome Group in the Seward Peninsula region of the Arctic Alaska–Chukotka terrane. Because recent plate reconstructions restore the Arctic Alaska–Chukotka terrane along northern Baltica during the early Paleozoic, the Alexander terrane might have comprised an arc system that fringed the Uralian continental margin.

ACKNOWLEDGMENTS

This is a product of the Geo-mapping for Energy and Minerals (GEM) program at Natural Resources Canada. D. Makkonen and S. Soubliere of TransNorth Turbo Air provided superb helicopter support in the Saint Elias Mountains. J. Strauss and A. Gould are thanked for their excellent field assistance. E. Spencer and B. Cousens are acknowledged for Sm-Nd isotope analyses at Carleton University. Insightful and constructive reviews by C. Soja, A. Till, and an anonymous reviewer improved this manuscript. This is Geological Survey of Canada publication 20110266.

REFERENCES CITED

Allègre, C. J.; Dupré, B.; Richard, P.; Rousseau, D.; and Brooks, C. 1982. Subcontinental versus suboceanic mantle, II: Nd-Sr-Pb isotopic comparison of continental tholeiites with mid-ocean ridge tholeiites, and the structure of the continental lithosphere. Earth Planet. Sci. Lett. 57:25–34.

Amato, J. M.; Toro, J.; Miller, E. L.; Gehrels, G. E.; Farmer, G. L.; Gottlieb, E. S.; and Till, A. B. 2009. Late Proterozoic–Paleozoic evolution of the Arctic Alaska–Chukotka terrane based on U-Pb igneous and detrital zircon ages: implications for Neoproterozoic paleogeographic reconstructions. Geol. Soc. Am. Bull. 121: 1219–1235.

Arculus, R. J., and Powell, R. 1986. Source component

mixing in the regions of arc magma generation. J. Geophys. Res. 91:5913–5926.

Ayuso, R. A., and Till, A. B. 2007. Geochemical and Nd-Pb isotopic evolution of metabasites from attenuated continental lithosphere, Nome Group, Seward Peninsula, Alaska. Geol. Soc. Am. Abstr. Progr. 39(6):489.

Bazard, D. R.; Butler, R. F.; Gehrels, G. E.; and Soja, C. M. 1995. Early Devonian paleomagnetic data from the lower Devonian Karheen Formation suggest Laurentia-Baltica connection for the Alexander terrane. Geology 23:707–710.

Berg, H. C.; Jones, D. L.; and Coney, P. J. 1978. Map showing pre-Cenozoic tectonostratigraphic terranes of southeastern Alaska and adjacent areas. U.S. Geol. Surv. Open File Rep. 78-1085.

Bjørlykke, A.; Vokes, F. M.; Birkeland, A.; and Thorpe, R. I. 1993. Lead isotope systematics of strata-bound sulfide deposits in the Caledonides of Norway. Econ. Geol. 88:397–417.

Blodgett, R. B.; Rohr, D. M.; and Boucot, A. J. 2002. Paleozoic links among some Alaskan accreted terranes and Siberia based on megafossils. *In* Miller, E. L.; Grantz, A.; and Klemperer, S., eds. Tectonic evolution of the Bering Shelf–Chukchi Sea–Arctic Margin and adjacent landmasses. Geol. Soc. Am. Spec. Pap. 360: 273–280.

Bradley, D. C. 2008. Passive margins through Earth history. Earth-Sci. Rev. 91:1–26.

Bradley, D. C.; McClelland, W. C.; Wooden, J. L.; Till, A. B.; Roeske, S. M.; Miller, M. L.; Karl, S. M.; and Abbott, J. G. 2007. Detrital zircon geochronology of some Neoproterozoic to Triassic rocks in interior Alaska. *In* Ridgway, K. D.; Trop, J. M.; Glen, J. M. G.; and O'Neill, J. M., eds. Tectonic growth of a collisional continental margin: crustal evolution of southern Alaska. Geol. Soc. Am. Spec. Pap. 431:155–189.

Busby, C. J., and Bassett, K. N. 2007. Volcanic facies architecture of an intra-arc strike-slip basin, Santa Rita Mountains, southern Arizona. Bull. Volcanol. 70:85–103.

Carter, C. 1977. Age of the Hood Bay Formation, Alaska. *In* Sohl, N. F., and Wright, W. B., eds., Changes in stratigraphic nomenclature by the U.S. Geological Survey, 1976. U.S. Geol. Surv. Bull. 1435-A, p. A117–A118.

Cawood, P. A.; Kröner, A.; Collins, W. J.; Kusky, T. M.; Mooney, W. A.; and Windley, B. F. 2009. Accretionary orogens through Earth history. *In* Cawood, P. A., and Kröner, A., eds., Earth accretionary systems in space and time. Geol. Soc. Lond. Spec. Publ. 318:1–36.

Cloos, M. 1993. Lithospheric buoyancy and collisional orogenesis: subduction of oceanic plateaus, continental margins, spreading ridges, and seamounts. Geol. Soc. Am. Bull. 105:715–737.

Cobbett, R.; Israel, S.; and Mortensen, J. K. 2010. The Duke River fault, southwest Yukon: preliminary examination of the relationships between Wrangellia and the Alexander terrane. Yukon Explor. Geol. 2009: 143–158.

Cocks, L. R. M., and Torsvik, T. H. 2005. Baltica from the late Precambrian to mid-Palaeozoic times: the gain and loss of a terrane's identity. Earth-Sci. Rev. 72:39–66.

———. 2007. Siberia, the wandering northern terrane, and its changing geography through the Palaeozoic. Earth-Sci. Rev. 82:29–74.

Colpron, M., and Nelson, J. L. 2009. A Palaeozoic Northwest Passage: incursion of Caledonian, Baltican and Siberian terranes into eastern Panthalassa, and the early evolution of the North American Cordillera. *In* Cawood, P. A., and Kröner, A., eds., Earth accretionary systems in space and time. Geol. Soc. Lond. Spec. Publ. 318:273–307.

Colpron, M.; Nelson, J. L.; and Murphy, D. C. 2007. Northern Cordilleran terranes and their interactions through time. GSA Today 17:4–10.

Coney, P. J.; Jones, D. L.; and Monger, J. W. H. 1980. Cordilleran suspect terranes. Nature 288:329–333.

Decker, J.; Bergman, S. C.; Blodgett, R. B.; Box, S. E.; Bundtzen, T. K.; Clough, J. G.; Conrad, W. L.; et al. 1994. Geology of southwestern Alaska. *In* Plafker, G., and Berg, H. C., eds. The geology of Alaska (Geology of North America, Vol. G-1). Boulder, CO, Geol. Soc. Am., p. 285–310.

DePaolo, D. J. 1981. Neodymium isotopes in the Colorado Front Range and crust-mantle evolution in the Proterozoic. Nature. 291:193–196.

———. 1988. Neodymium isotope geochemistry: an introduction. New York, Springer, 187 p.

Dodds, C. J., and Campbell, R. B. 1992. Overview, legend, and mineral deposit tabulations for geology of SW Kluane Lake (115G & F[E1/2]), Mount Saint Elias (115B & C[E1/2]), SW Dezadeash (115A), NE Yakutat (114O), and Tatshenshini (114P) map areas, Yukon Territory and British Columbia. Geol. Surv. Can. Open Files 2188–2191, 85 p.

Dodds, C. J.; Campbell, R. B.; Read, P. B.; Orchard, M. J.; Tozer, E. T.; Bamber, E. W.; Pedder, A. E. H.; et al. 1993. Macrofossil and conodont data from SW Kluane Lake (115G & F[E1/2]), Mount Saint Elias (115B & C[E1/2]), SW Dezadeash (115A), NE Yakutat (114O), and Tatshenshini (114P) map areas, Yukon Territory and British Columbia. Geol. Surv. Can. Open File 2731, 137 p.

Dumoulin, J. A.; Harris, A. G.; Gagiev, M.; Bradley, D. C.; and Repetski, J. E. 2002. Lithostratigraphic, conodont, and other faunal links between lower Paleozoic strata in northern and central Alaska and northeastern Russia. *In* Miller, E. L.; Grantz, A.; and Klemperer, S., eds., Tectonic evolution of the Bering Shelf–Chukchi Sea–Arctic Margin and adjacent landmasses. Geol. Soc. Am. Spec. Pap. 360:291–312.

Eberlein, G. D., and Churkin, M., Jr. 1970. Paleozoic stratigraphy in the northwest coastal area of Prince of Wales Island, southeastern Alaska. U.S. Geol. Surv. Bull. 1284, 67 p.

Escuder Viruete, J.; Contreras, F.; Stein, G.; Urien, P.; Joubert, M.; Pérez-Estaún; Friedman, R.; and Ullrich, T. 2007. Magmatic relationships and ages between adakites, magnesian andesites and Nb-enriched

basalt-andesites from Hispaniola: record of major change in the Caribbean island arc magma sources. Lithos 99:151–177.

Fitton, J. G. 2007. The OIB paradox. *In* Foulger, G. R., and Jurdy, D. M., eds., Plates, plumes, and planetary processes. Geol. Soc. Am. Spec. Pap. 430:387–412.

Gehrels, G. E. 1990. Late Proterozoic-Cambrian metamorphic basement to the Alexander terrane on Long and Dall Islands, southeastern Alaska. Geol. Soc. Am. Bull. 102:760–767.

Gehrels, G. E., and Berg, H. C. 1992. Geologic map of southeastern Alaska. U.S. Geol. Surv. Miscellaneous Geologic Investigations Map I-1867, 24, p.

Gehrels, G. E.; Butler, R. F.; and Bazard, D. R. 1996. Detrital zircon geochronology of the Alexander terrane, southeastern Alaska. Geol. Soc. Am. Bull. 108:722–734.

Gehrels, G. E., and Saleeby, J. B. 1987*a*. Geologic framework, tectonic evolution, and displacement history of the Alexander terrane. Tectonics 6:151–173.

———. 1987*b*. Geology of southern Prince of Wales Island, southeastern Alaska. Geol. Soc. Am. Bull. 98: 123–137.

Goldstein, S. L.; O'Nions, R. K.; and Hamilton, P. J. 1984. A Sm-Nd isotopic study of atmospheric dusts and particulates from major river systems. Earth Planet. Sci. Lett. 70:221–236.

Gordey, S. P., and Makepeace, A. J. 2003. Yukon digital geology, version 2.0. Geol. Surv. Can. Open File 1749, CD-ROM.

Gorring, M. L., and Kay, S. 2001. Mantle processes and sources of Neogene slab window magmas from southern Patagonia, Argentina. J. Petrol. 42:1067–1094.

Gradstein, F.; Ogg, J.; and Smith, A. 2004. A geologic time scale 2004. Cambridge, Cambridge University Press.

Grenne, T.; Ihlen, P. M.; and Vokes, F. M. 1999. Scandinavian Caledonide metallogeny in a plate tectonic perspective. Min. Depos. 34:422–471.

Grove, M.; Gehrels, G. E.; Cotkin, S. J.; Wright, J. E.; and Zou, H. 2008. Non-Laurentian cratonal provenance of Late Ordovician eastern Klamath blueschists and a link to the Alexander terrane. *In* Wright, J. E., and Shervais, J. W., eds. Ophiolites, arcs, and batholiths. Geol. Soc. Am. Spec. Pap. 438:223–250.

Hawkesworth, C. J.; Kempton, P. D.; Rogers, N. W.; Ellam, R. M.; and van Calsteren, P. W. 1990. Continental mantle lithosphere, and shallow level enrichment processes in the Earth's mantle. Earth Planet. Sci. Lett. 96:256–268.

Hawkins, J. W. 1995. The geology of the Lau Basin. *In* Taylor, B., ed. Backarc basins: tectonics and magmatism. New York, Plenum, p. 63–138.

Hochstaedter, A. G.; Gill, J. B.; and Morris, J. D. 1990. Volcanism in the Sumisu Rift, II: subduction and nonsubduction related components. Earth Planet. Sci. Lett. 100:195–209.

Huang, C.-H.; Yuan, P. B.; and Tsao, S.-H. 2006. Temporal and spatial records of active arc-continent collision in Taiwan: a synthesis. Geol. Soc. Am. Bull. 118:274–288.

Israel, S. 2004. Geology of southwestern Yukon. Yukon Geol. Surv. Open File 2004-16, scale 1 : 250,000.

Jenner, G. A. 1996. Trace element geochemistry of igneous rocks: geochemical nomenclature and analytical geochemistry. *In* Wyman, D. A., ed. Trace element geochemistry of volcanic rocks: applications for massive sulphide exploration. Geol. Assoc. Can. Short Course Notes 12:51–77.

Karl, S. M.; Haeussler, P. J.; Friedman, R. M.; Mortensen, J. K.; Himmelberg, G. R.; and Zumsteg, C. L. 2006. Late Proterozoic ages for rocks on Mount Cheetdeekahyu and Admiralty Island, Alexander terrane, southeast Alaska. Geol. Soc. Am. Abstr. Progr. 38(5): 20.

Karl, S. M.; Layer, P. W.; Harris, A. G.; Haeussler, P. J.; and Murchey, B. L. 2010. The Cannery Formation: Devonian to Early Permian arc-marginal deposits within the Alexander terrane, southeastern Alaska. *In* Dumoulin, J. A., and Galloway, J. P., eds. Studies by the U.S. Geological Survey in Alaska 2008–2009. U.S. Geol. Surv. Prof. Pap. 1776-B, 45 p.

Kepezhinskas, P.; McDermott, F.; Defant, M. J.; Hochstaedter, A.; Drummond, M. S.; Hawkesworth, C. J.; Koloskov, A.; Maury, R. C.; and Bellon, H. 1997. Trace element and Sr-Nd-Pb isotopic constraints on a three-component model of Kamchatka arc petrogenesis. Geochim. Cosmochim. Acta 61:577–600.

Kobayashi, K.; Kasuga, S.; and Okino, K. 1995. Shikoku Basin and its margins. *In* Taylor, B., ed. Backarc basins: tectonics and magmatism. New York, Plenum, p. 381–405.

Kuzmichev, A.; Kröner, A.; Hegner, E.; Liu, D.; and Wang, Y. 2005. The Shishkhid ophiolite, northern Mongolia: a key to the reconstruction of a Neoproterozoic island-arc system in central Asia. Precambrian Res. 138:125–150.

Lindsley-Griffin, N.; Griffin, J. R.; and Farmer, J. D. 2008. Paleogeographic significance of Ediacaran cyclomedusoids within the Antelope Mountain Quartzite, Yreka terrane, eastern Klamath Mountains, California. *In* Blodgett, R. B., and Stanley, G. D., Jr., eds. The terrane puzzle: new perspectives on paleontology and stratigraphy from the North American Cordillera. Geol. Soc. Am. Spec. Pap. 442:1–37.

MacLean, W. H., and Barrett, T. J. 1993. Lithogeochemical techniques using immobile elements. J. Geochem. Explor. 48:109–133.

McClelland, W. C., and Gehrels, G. E. 1990. Geology of the Duncan Canal shear zone: evidence for Early to Middle Jurassic deformation of the Alexander terrane, southeastern Alaska. Geol. Soc. Am. Bull. 102:1378–1392.

McDonough, W. F., and Sun, S.-s. 1995. The composition of the Earth. Chem. Geol. 120:223–253.

McPhie, J. 1995. A Pliocene shoaling basaltic seamount: Ba Volcanic Group at Rakiraki, Fiji. J. Volcanol. Geotherm. Res. 64:193–210.

McPhie, J., and Allen, R. L. 1992. Facies architecture of mineralized submarine volcanic sequences: Cambrian

Mount Read Volcanics, western Tasmania. Econ. Geol. 87:587–596.
Mihalynuk, M. G.; Smith, M. T.; MacIntyre, D. G.; and Deschênes, M. 1993. Tatshenshini project, part B: stratigraphic and magmatic setting of mineral occurrences. British Columbia Ministry of Energy, Mines, and Petroleum Resources Paper 1993-1:189–228.
Miller, E. L.; Gehrels, G. E.; Pease, V.; and Sokolov, A. 2010. Paleozoic and Mesozoic stratigraphy and U-Pb detrital zircon geochronology of Wrangel Island, Russia: constraints on paleogeography and paleocontinental reconstructions of the Arctic. Am. Assoc. Petrol. Geol. Bull. 94:665–692.
Miller, E. L.; Kuznetsov, N.; Soboleva, A.; Udoratina, O.; Grove, M. J.; and Gehrels, G. E. 2011. Baltica in the Cordillera? Geology 39:791–794.
Molnar, P., and Atwater, T. 1978. Interarc spreading and Cordilleran tectonics as related to the age of subducted oceanic lithosphere. Earth Planet. Sci. Lett. 41: 330–340.
Monger, J. W. H., and Nokelberg, W. J. 1996. Evolution of the northern North American Cordillera: generation, fragmentation, displacement and accretion of successive North America plate-margin arcs. *In* Coyner, A. R., and Fahey, P. L., eds. Geology and ore deposits of the American Cordillera, Geological Society of Nevada Symposium Proceedings, Reno/ Sparks, Nevada, April 1995, Vol. 3, p. 1133–1152.
Nelson, J. L.; Diakow, L. J.; Karl, S.; Mahoney, J. B.; Gehrels, G. E.; Pecha, M.; and van Staal, C. R. 2010. Geology and mineral potential of the southern Alexander terrane and western coast plutonic complex near Klemtu, northwestern British Columbia. British Columbia Ministry of Energy, Mines, and Petroleum Resources Geological Fieldwork Paper 2011-1, p. 73–98.
Nikishin, A. M.; Ziegler, P. A.; Stephenson, R. A.; Cloetingh, S. A. P. L.; Fume, A. V.; Fokin, P. A.; Ershov, A. V.; et al. 1996. Late Precambrian to Triassic history of the East European Craton: dynamics of sedimentary basin evolution. Tectonophysics 268:23–63.
Norford, B. S., and Mihalynuk, M. G. 1994. Evidence of the Pacific Faunal Province in the northern Alexander Terrane, recognition of two Middle Ordovician graptolite zones in northwestern British Columbia. Can. J. Earth Sci. 31:1389–1396.
Palmer, A. R. 1983. The decade of North American geology 1983 time scale. Geology 11:503–504.
Pavlis, T. L.; Picornell, C.; Serpa, L.; Bruhn, R. L.; and Plafker, G. 2004. Tectonic processes during oblique collision: insights from the St. Elias orogen, northern North American Cordillera. Tectonics 23:TC3001.
Pearce, J. A. 1996. A user's guide to basalt discrimination diagrams. *In* Wyman, D. A., ed. Trace element geochemistry of volcanic rocks: applications for massive sulphide exploration. Geol. Assoc. Can. Short Course Notes 12:79–113.
Pearce, J. A., and Cann, J. R. 1973. Tectonic setting of basic volcanic rocks determined using trace element analyses. Earth Planet. Sci. Lett. 19:290–300.
Pearce, J. A., and Peate, D. W. 1995. Tectonic implications of the composition of volcanic arc magmas. Annu. Rev. Earth Planet. Sci. 23:251–285.
Peate, D. W.; Pearce, J. A.; Hawkesworth, C. J.; Colley, H.; Edwards, C. M. H.; and Hirose, K. 1997. Geochemical variations in Vanuatu arc lavas: the role of subducted material and a variable mantle wedge composition. J. Petrol. 38:1331–1358.
Piercey, S. J.; Murphy, D. C.; Mortensen, J. K.; and Creaser, R. A. 2004. Mid-Paleozoic initiation of the northern Cordilleran marginal backarc basin: geologic, geochemical, and neodymium isotope evidence from the oldest mafic magmatic rocks in the Yukon-Tanana terrane, Finlayson Lake district, southeast Yukon, Canada. Geol. Soc. Am. Bull. 116:1087–1106.
Piercey, S. J.; Nelson, J. L.; Colpron, M.; Dusel-Bacon, C.; Simard, R.-L.; and Roots, C. F. 2006. Paleozoic magmatism and crustal recycling along the ancient Pacific margin of North America, northern Cordillera. *In* Colpron, M., and Nelson, J. L., eds. Paleozoic evolution and metallogeny of pericratonic terranes at the ancient Pacific margin of North America, Canadian and Alaskan Cordillera. Geol. Assoc. Can. Spec. Pap. 45: 281–322.
Pisarevsky, S. A.; Murphy, J. B.; Cawood P. A.; and Collins, A. S. 2008. Late Neoproterozoic and Early Cambrian palaeogeography: models and problems. *In* Pankhurst, R. J.; Trouw, R. A. J.; de Brito Neves, B. B.; and de Wit, M. J., eds. West Gondwana: pre-Cenozoic correlations across the South Atlantic region. Geol. Soc. Lond. Spec. Publ. 294:9–31.
Pouclet, A.; Lee, J-S.; Vidal, P.; Cousens, B.; and Bellon, H. 1995. Cretaceous to Cenozoic volcanism in South Korea and in the Sea of Japan: magmatic constraints on the opening of the back-arc basin. *In* Smellie, J. L., ed. Volcanism associated with extension at consuming plate margins. Geol. Soc. Lond. Spec. Publ. 81:169–191.
Rogers, G., and Hawkesworth, C. J. 1989. A geochemical traverse across the northern Chilean Andes: evidence for crust generation from the mantle wedge. Earth Planet. Sci. Lett. 91:271–285.
Samson, S. D.; Barr, S. M.; and White, C. E. 1995. Nd isotopic characteristics of terranes within the Avalon Zone, southern New Brunswick. Can. J. Earth Sci. 37: 1039–1052.
Samson, S. D.; McClelland, W. C.; Patchett, P. J.; Gehrels, G. E.; and Anderson, R. G. 1989. Evidence from neodymium isotopes for mantle contributions to Phanerozoic crustal genesis in the Canadian Cordillera. Nature 337:705–709.
Shervais, J. W. 1982. Ti-V plots and the petrogenesis of modern and ophiolitic lavas. Earth Planet. Sci. Lett. 59:101–118.
Shinjo, R.; Chung, S.-L.; Kato, Y.; and Kimura, M. 1999. Geochemical and Sr-Nd isotopic characteristics of volcanic rocks from the Okinawa Trough and Ryukyu arc: implications for the evolution of a young, intracontinental back arc basin. J. Geophys. Res. 104: 10591–10608.
Shinjo, R.; Woodhead, J. D.; and Hergt, J. M. 2000. Geo-

chemical variation within the northern Ryukyu arc: magma source compositions and geodynamic implications. Contrib. Mineral. Petrol. 140:263–282.

Slack, J. F.; Shanks, W. C.; Karl, S. M.; Gemery, P. A.; Bittenbender, P. E.; and Ridley, W. I. 2006. Geochemical and sulfur-isotopic signatures of volcanogenic massive sulfide deposits on Prince of Wales Island and vicinity, southeastern Alaska. U.S. Geol. Surv. Prof. Pap. 1732-C, 37 p.

Soja, C. M. 1990. Island arc carbonates from the Silurian Heceta Formation of southeastern Alaska (Alexander terrane). J. Sediment. Petrol. 60:235–249.

———. 1994. Significance of Silurian stromatolite-sphinctozoan reefs. Geology 22:355–358.

———. 2008. Silurian-bearing terranes of Alaska. *In* Blodgett, R. B., and Stanley, G. D., Jr., eds. The terrane puzzle: new perspectives on paleontology and stratigraphy from the North American Cordillera. Geol. Soc. Am. Spec. Pap. 442:39–50.

Soja, C. M., and Antoshkina, A. I. 1997. Coeval development of Silurian stromatolite reefs in Alaska and the Ural Mountains: implications for paleogeography of the Alexander terrane. Geology 25:539–542.

Soja, C. M., and Krutikov, L. 2008. Provenance, depositional setting, and tectonic implications of Silurian polymictic conglomerate in Alaska's Alexander terrane. *In* Blodgett, R. B., and Stanley, G. D., Jr., eds. The terrane puzzle: new perspectives on paleontology and stratigraphy from the North American Cordillera. Geol. Soc. Am. Spec. Pap. 442:63–75.

Stolz, A. J.; Varne, R.; Davies, G. R.; Wheller, G. E.; and Foden, J. D. 1990. Magma source components in an arc-continent collision zone: the Flores-Lembata sector, Sunda arc, Indonesia. Contrib. Mineral. Petrol. 105:585–601.

Sun, S.-s., and McDonough, W. F. 1989. Chemical and isotopic systematics of oceanic basalts: implications for mantle composition and processes. *In* Saunders, A. D., and Norry, M. J., eds. Magmatism in ocean basins. Geol. Soc. Lond. Spec. Publ. 42:313–345.

Swinden, H. S.; Jenner, G. A.; Fryer, B. J.; Hertogen, J.; and Roddick, J. C. 1990. Petrogenesis and paleotectonic history of the Wild Bight Group, an Ordovician rifted island arc in central Newfoundland. Contrib. Mineral. Petrol. 105:219–241.

Taylor, B.; Brown, G.; Fryer, P.; Gill, J. B.; Hochstaedter, A. G.; Hotta, H.; Langmuir, C. H.; Lenien, M.; Nishimura, A.; and Urabe, T. 1990. Alvin-SeaBeam studies of the Sumisu Rift, Izu-Bonin arc. Earth Planet. Sci. Lett. 100:127–147.

Till, A. B., and Dumoulin, J. A. 1994. Geology of Seward Peninsula and Saint Lawrence Island. *In* Plafker, G., and Berg, H. C., eds. The geology of Alaska (Geology of North America, Vol. G-1). Boulder, CO, Geol. Soc. Am., p. 141–152.

Till, A. B.; Dumoulin, J. A.; and Bradley, D. C. 2010. Paleogeographic reconstruction of the Arctic Alaska–Chukotka terrane based on zircon and paleontologic data from Seward Peninsula. Geol. Soc. Am. Abstr. 42(5):573.

van Staal, C. R.; Barr, S. M.; Hibbard, J.; Murphy, J. B.; and McCausland, P. J. A. 2011. The tectonic evolution of Laurentia and West Gondwana from 600–400 Ma: an Appalachian-Caledonian perspective. *In* Schmitt, R. S.; Trouw, R.; Carvalho, I. S.; and Collins, A., eds. Abstracts, Gondwana 14: Reuniting Gondwana: East Meets West, Búzios, Brazil, September 25–30. Rio de Janeiro, Universidade Federal do Rio de Janeiro, p. 142.

van Staal, C. R.; Beranek, L. P.; Israel, S. A.; McClelland, W. C.; Mihalynuk, M. G.; Nelson, J. L.; and Joyce, N. 2010. New ideas on the Paleozoic-Triassic evolution of the Insular superterrane of the North American Cordillera. Geol. Soc. Am. Abstr. 42(5):574.

van Staal, C. R.; Winchester, J. A.; and Bédard, J. H. 1991. Geochemical variations in Middle Ordovician volcanic rocks of the northern Miramichi Highlands and their tectonic significance. Can J. Earth Sci. 28:1031–1049.

Wang, K.-L.; Chung, S.-L.; Chen, C.-H.; and Chen, C.-H. 2002. Geochemical constraints on the petrogenesis of high-Mg basaltic andesites from the Northern Taiwan Volcanic Zone. Chem. Geol. 182:513–528.

Wang, K.-L.; Chung, S.-L.; Chen, C.-H.; Shinjo, R.; Yang, T. F.; and Chen C.-H. 1999. Post-collisional magmatism around northern Taiwan and its relation with opening of the Okinawa Trough. Tectonophysics 308: 363–376.

Winchester, J. A., and Floyd, P. A. 1977. Geochemical discrimination of different magma series and their differentiation products using immobile elements. Chem. Geol. 20:325–343.

Wood, D. A. 1980. The application of a Th-Hf-Ta diagram to problems of tectonomagmatic classification and to establishing the nature of crustal contamination of basaltic lavas of the British Tertiary Volcanic Province. Earth Planet. Sci. Lett. 50:11–30.

Wright, J. E., and Wyld, S. J. 2006. Gondwanan, Iapetan, Cordilleran interactions: a geodynamic model for the Paleozoic tectonic evolution of the North American Cordillera. *In* Haggart, J. W.; Enkin, R. J.; and Monger, J. W. H., eds. Paleogeography of the North American Cordillera: evidence for and against large-scale displacements. Geol. Assoc. Can. Spec. Pap. 46:377–408.

Table A1 – Beranek et al.

Lithofacies	Characteristics	Contact relationships and associated lithofacies	Interpretation
Basaltic facies association			
Massive basalt	4-23 m-thick, >500 m in lateral extent; 60% aphyric to vesicular to amygdaloidal basalt, 40% crowded to evenly porphyritic basalt with 1-10 mm tabular to equant plagioclase phenocrysts; locally columnar jointed.	Upper and lower contacts are conformable to subconformable and typically juxtaposed with sediment-matrix basalt breccia lithofacies; frothy textures and tubular- to irregular-shaped pipe vesicles locally occur along contacts with silty limestone and fossiliferous sandstone lithofacies.	Coherent lava, emplaced by flows or sills; sills distinguished primarily based on peperite texture at upper contact.
Pillow basalt (Figures 7A, 7B)	5-10 m-thick, >500 m in lateral extent; 0.25-5.0 m closely packed lobes; wormy to glassy lobe margins; 50% aphyric vesicular basalt, 50% vesicular basalt porphyry; locally contains interpillow matrix of light grey limestone.	Upper and lower contacts are conformable with clast-supported monomictic basalt breccia and fossiliferous sandstone lithofacies; pillowed horizons laterally grade into the massive basalt lithofacies.	Pillowed lava flows in subaqueous environment (Moore 1975).
Sediment-matrix basalt breccia (Figures 7C, 7D)	<2 m-thick, non-stratified, poorly sorted; carbonate and lithic sand matrix; lapilli- to block-sized clasts of amoeboid, oblate, and angular basalt that are detached from adjacent coherent facies.	Locally occurs at lower contact and less commonly upper contact of massive basalt in contact with sandstone. Contact characterized by rafts of laminated sandstone within locally highly vesicular ("frothy") massive basalt.	Emplacement of lava into/onto saturated sediment, creating fluidal to blocky peperite (e.g., Skilling et al. 2002).
Volcanogenic sedimentary facies association			
Well-stratified sandstone and conglomerate (Figure 8A)	<15 m-thick, >500 m in lateral extent; thin- to medium-bedded, fine- to coarse-grained, planar laminated to planar to trough cross-bedded (small-scale, ~4 cm-thick), moderately well sorted, calcareous, feldspathic lithic sandstone; local 4-15 cm-thick packages of normally graded 1-3 cm-thick couplets with coarse- to fine-grained sandstone and minor argillaceous carbonate; <10 m-thick, thick-bedded to crudely bedded, matrix-supported, moderately to well-sorted, planar to trough cross-bedded (large-scale, ~45 cm-thick) granule to pebble conglomerate; well-rounded to subangular clasts of texturally diverse basalt; matrix composed of calcareous lithic sandstone.	Sharp to intermingled contact with massive and pillow basalt lithofacies.	High-energy reworking of volcaniclastic gravel in shallow-marine depositional regime; graded packages may be evidence of turbidity current deposits.
Monomictic basalt breccia (Figure 8B)	<5 m-thick; chaotic horizons comprise non-stratified, poorly sorted, lapilli- to block-sized pillow fragments; medium-bedded units consist of angular, lapilli-sized clasts of vesicular to aphyric basalt with curviplanar margins.	Depositionally overlies pillow basalt lithofacies.	*In situ* to partly and wholly resedimented hyaloclastite (Batiza and White 2000), formed from proximal disintegration of quench fragmentated lava in contact with water.
Massive to weakly graded conglomerate (Figure 8C)	<10 m-thick, massive to weakly graded, matrix-supported, very poorly sorted; well-rounded to subangular, pebble- to boulder-sized clasts of texturally diverse basalt and volcaniclastic rocks; matrix composed of calcareous volcaniclastic sand (feldspar, basalt lithics).	Scoured lower contacts with underlying units of the volcanogenic sedimentary and limestone-sandstone facies associations. Locally observed to grade upwards into silty limestone and well-stratified sandstone and conglomerate.	High particle concentration debris flow deposit; gravity-driven collapse of volcaniclastic gravel that previously resided in high-energy, nearshore environment.
Limestone-sandstone facies association			
Silty limestone	<6 m-thick, thin- to medium-bedded.	Sharp to intermingled lower and upper contacts with massive basalt and pillow basalt lithofacies.	Suspension sedimentation of carbonate and fine-grained clastic input below wave-base.
Fossiliferous sandstone	<15 m-thick, fine- to medium-grained, thin- to medium-bedded, parallel laminated in part, calcareous, feldspathic sandstone; tabular geometry; yields brachiopod fossils.	Sharp to intermingled lower contact with massive basalt lithofacies; upper depositional contact with pillow basalt lithofacies.	Low-energy shelf environment.

Table A2

Suite/Sample No.	Sample I-1	Sample I-2	Sample I-3	Sample I-4	Sample I-5	Sample I-6	Sample I-7	Sample I-8	Sample I-9	Sample I-10
Field Collection No.	10VLB05	10VLB06	10VLB07	10VLB10	10VLB13	10VLB14	10VLB16	10VLB02	10VLB19	10VLB20
Easting (NAD 83)	342055	341899	341789	341402	341345	341462	341422	341996	339248	339321
Northing (NAD83)	6675522	6674982	6674894	6674664	6674682	6674285	6674256	6673363	6677911	6679017
SiO_2 (wt.%)	48.74	51.17	47.41	46	48.61	49.21	48.57	48.12	49.82	48.42
TiO_2	3	1.15	1.26	1.2	3.21	1.9	3.38	2.52	2.68	1.52
Al_2O_3	14.63	18	21	20.35	13.8	15.93	13.64	14.63	14.6	17.51
Fe_2O_3t	14.15	7.82	8.97	8.51	15.09	10.85	14.84	11.45	14.35	9.05
MnO	0.198	0.108	0.156	0.128	0.202	0.188	0.218	0.177	0.23	0.14
MgO	4.14	5.15	4.69	4.62	3.98	6.92	3.91	3.19	4.29	6.99
CaO	7.78	8.63	7.83	11.63	8.19	6.39	8.43	8.35	7.11	8.34
Na_2O	3.66	4.75	3.22	2.77	3.68	3.63	4.18	3.56	3.98	4.12
K_2O	0.39	0.4	2.08	0.06	0.23	1.72	0.17	1.27	0.73	0.37
P_2O_5	0.38	0.13	0.15	0.13	0.4	0.19	0.48	0.39	0.34	0.22
LOI	2.29	2.96	3.96	4.38	2.25	3.65	2.25	2.93	2.29	3.76
TOTAL	99.37	100.3	100.7	99.79	99.64	100.6	100.1	100.4	100.4	100.5
Sc (ppm)	36	27	27	29	37	38	37	26	37	33
V	344	190	205	208	434	336	334	237	387	222
Cr	< 20	120	30	80	< 20	110	< 20	< 20	< 20	170
Co	34	23	28	29	32	40	33	24	36	33
Ni	40	40	40	40	30	60	30	40	30	90
Y	51.5	20.6	20.8	20.6	45	35.7	52.2	42.4	42.9	27.9
Zr	256	90	89	91	218	190	259	219	197	135
Hf	5.8	2	2.2	2.1	4.8	4.3	5.5	4.9	4.6	3.1
Nb	16	5.7	5	6.6	14.5	10	17.9	13.8	10.9	9.1
Ta	0.79	0.1	0.12	0.13	0.71	0.47	0.93	0.75	0.57	0.27
Th	2.64	1.04	1.01	0.96	2.15	1.75	2.53	2.16	1.67	1.34
U	0.86	0.32	0.12	0.25	0.76	0.56	0.97	0.67	0.61	0.41
La	19.8	8.94	8.34	8.63	17.8	13.2	21.4	18.4	15.9	14.1
Ce	48.2	19.3	20.5	20.5	42.8	32.6	51.2	44.3	39.1	34.8
Pr	6.48	2.42	2.68	2.69	5.87	4.36	6.89	5.84	5.27	4.58
Nd	29	10.6	11.6	11.6	26.2	19.5	30.7	26.2	23.5	19.2
Sm	7.87	2.85	3.14	3.06	7.19	5.3	8.05	6.95	6.47	4.46
Eu	2.52	1.12	1.19	1.12	2.46	1.48	2.72	2.29	2.21	1.5
Gd	8.81	3.4	3.54	3.48	7.72	5.93	8.97	7.65	7.6	4.77
Tb	1.51	0.6	0.62	0.61	1.35	1.04	1.54	1.3	1.33	0.81
Dy	9.27	3.65	3.86	3.75	8.06	6.29	9.27	7.74	7.97	4.98
Ho	1.84	0.71	0.78	0.73	1.57	1.25	1.82	1.53	1.6	1.01
Er	5.29	2.01	2.19	2.03	4.48	3.63	5.2	4.37	4.55	2.9
Tm	0.778	0.289	0.319	0.295	0.649	0.538	0.762	0.63	0.673	0.428
Yb	5	1.88	2.06	1.94	4.15	3.61	4.88	4.09	4.37	2.81
Lu	0.781	0.313	0.325	0.323	0.655	0.576	0.76	0.641	0.7	0.448
Mg#	38	58	52	53	36	57	36	37	38	61

Table A2

Suite/Sample No.	Sample I-11	Sample II-1	Sample II-2	Sample III-1	Sample III-2	Sample III-3	Sample III-4	Sample III-5	Sample III-6	Sample III-7
Field Collection No.	09VL45	09VL01	10VLB22	09VLB39	09VL44	MMI92-33-1	MMI92-181	MMI92-18-4	09VL07	MSM92-186
Easting (NAD 83)	342916	634813	339929	502158	337179	352325	339500	341025	340918	343400
Northing (NAD83)	6654499	6741723	6679825	6781211	6661606	6651400	6650500	6651850	6652000	6639550
SiO_2 (wt.%)	50.5	50.4	55.05	47.87	49.63	47.89	50.41	47.42	46.61	45.03
TiO_2	3.31	0.95	1.85	2.75	1.76	3.13	2.93	2.4	2.43	1.88
Al_2O_3	12.22	19.59	12.49	14.98	17.71	13.47	12.89	13.46	13.57	15.46
Fe_2O_3t	15.02	8.77	14.44	11.87	10.57	14.61	11.66	13.63	13.81	12.18
MnO	0.187	0.148	0.347	0.175	0.14	0.18	0.17	0.19	0.224	0.2
MgO	4.18	3.29	1.99	6.26	4.98	5.39	3.82	6.77	6.65	7.62
CaO	6.78	4.51	5.33	10.27	9.31	8.02	8.6	8.26	8.91	9.12
Na_2O	4.64	5.41	4.36	3.08	4.15	3.3	4.55	4.06	3.56	2.42
K_2O	0.07	1.36	0.54	0.44	0.15	0.92	0.29	0.08	0.17	1.15
P_2O_5	0.65	0.51	0.85	0.35	0.29	0.44	0.7	0.3	0.32	0.25
LOI	2.21	3.84	2.7	2.3	0.89	2.39	3.52	3.3	2.95	4.32
TOTAL	99.77	98.78	99.95	100.3	99.59	99.74	99.54	99.87	99.21	99.63
Sc (ppm)	33	6	33	28	27	NA	NA	NA	27	NA
V	338	211	20	264	215	NA	NA	NA	205	NA
Cr	< 20	< 20	< 20	150	40	NA	NA	NA	30	NA
Co	31	23	9	41	31	NA	NA	NA	28	NA
Ni	< 20	< 20	< 20	90	30	NA	NA	NA	40	NA
Y	63.1	30.7	62	27.8	27.6	31.8	38.8	35.5	20.8	22.59
Zr	352	159	209	206	172	244	246	154	89	121
Hf	7.7	3.4	4.7	4.5	3.6	6.4	5.69	3.87	2.2	3.2
Nb	22	11.4	12.9	17.7	16.8	19.1	24.7	9.18	5	11.4
Ta	1.53	0.84	0.57	1.24	1.16	0.974	1.46	0.562	0.12	0.704
Th	2.7	6.87	2.5	1.32	1.6	1.93	1.94	0.776	1.01	1.08
U	1.05	2.92	0.79	0.45	0.54	NA	NA	NA	0.12	NA
La	27.6	36.6	22.9	17.3	17.7	19.9	24.3	9.59	8.34	12.2
Ce	65.8	78.7	59.1	40.7	39.5	47.1	60.1	25	20.5	28.1
Pr	9.31	9.73	8.35	5.79	5.27	6.6	8.32	3.77	2.68	3.87
Nd	42	39.3	39.4	26.2	22	31.3	38.3	19.1	11.6	17.2
Sm	10.7	8.75	10.7	6.91	5.39	7.62	9.28	5.72	3.14	4.65
Eu	3.06	2.42	4.36	2.14	1.73	2.77	3.52	1.81	1.19	1.58
Gd	11.1	7.12	11.7	6.19	5.2	8.3	10.3	7.14	3.54	5.01
Tb	1.94	1.14	1.96	1	0.89	1.2	1.3	1.04	0.62	0.721
Dy	11.2	6.08	11.4	5.44	5.11	7.78	8.46	7.13	3.86	4.74
Ho	2.15	1.11	2.15	0.96	0.95	1.47	1.56	1.42	0.78	0.891
Er	6.09	3.15	6.04	2.53	2.62	3.94	4.16	4.01	2.19	2.5
Tm	0.881	0.458	0.885	0.34	0.382	0.508	0.557	0.559	0.319	0.35
Yb	5.84	2.87	5.75	2.07	2.44	3.048	3.2	3.47	2.06	2.2
Lu	0.913	0.446	0.911	0.299	0.384	0.445	0.49	0.491	0.325	0.321
Mg#	37	44	22	52	50	44	41	51	50	57

Table A3

Sample No.	Field Collection No.	Age (Ma)	Sm (ppm)	Nd (ppm)	$^{143}Nd/^{144}Nd_m$	$^{143}Nd/^{144}Nd_i$	$^{147}Sm/^{144}Nd$	$\varepsilon Nd_{(i)}$	T_{DM} (Ma)
Sample I-11	09VL45	488	10.4	40	0.512782(14)	0.512279	0.1572	+ 5.2	894
Sample II-1	09VL01	488	8.03	36.3	0.512673(16)	0.512245	0.1338	+ 4.6	840
Sample III-1	09VLB39	488	6.66	25.80	0.512699(15)	0.512201	0.1559	+ 3.7	1091
Sample III-2	09VL44	488	5.39	22.2	0.512727(15)	0.512258	0.1466	+ 4.8	878
Sample III-6	09VL07	488	5.96	20.1	0.512880(15)	0.512308	0.1791	+ 5.8	1026